FINAL REPORT

CHARACTERIZATION OF DRAINAGE LAYER PROPERTIES FOR MECHANISTIC-EMPRIRICAL PAVEMENT DESIGN

Linbing Wang, Ph.D., P.E.
Professor
Via Department of Civil and Environmental Engineering
Virginia Polytechnic Institute and State University
Blacksburg, Virginia

Yinning Zhang, Ph.D.
Graduate Research Assistant
Via Department of Civil and Environmental Engineering
Virginia Polytechnic Institute and State University
Blacksburg, Virginia

Brian K. Diefenderfer, Ph.D., P.E.
Associate Principal Research Scientist
Virginia Transportation Research Council
Charlottesville, Virginia

Benjamin F. Bowers, Ph.D.
Research Scientist
Virginia Transportation Research Council
Charlottesville, Virginia

Transportation Pooled Fund Study TPF-5(229)

June 2016

ABSTRACT

The structural performance of the drainage layer within a pavement is unclear and has not always been considered in pavement design procedures in the past, which may lead to structural problems in the pavement. The structural performance of pavement drainage layers are not always considered in the pavement design process. The objective of this project was to characterize the properties of typically adopted drainage layer materials in Virginia, Oklahoma, Idaho, and Wisconsin, and incorporate these drainage layer properties into mechanistic-empirical pavement design procedures. A series of laboratory tests were conducted to quantify the volumetric properties, permeability and mechanical properties of laboratory-compacted asphalt treated, cement treated, and unbound permeable base specimens. A modified dynamic modulus test protocol was developed for project-specific materials characterization inputs and the calibrated NCHRP 1-37A model was used to provide more general characterization values as level 2 input for asphalt stabilized drainage layer materials. The compressive strength of the cement treated permeable base mixture was also quantified through testing. Laboratory tests and numerical simulations were conducted to investigate the resilient modulus of unbound drainage layer materials. The location effects and the structural contribution of the drainage layer were investigated by finite-element method analysis. The optimal air void content of the drainage layer was determined based on the laboratory-measured permeability and the predicted pavement performance during a theoretical 20-year service life.

FINAL REPORT

CHARACTERIZATION OF DRAINAGE LAYER PROPERTIES FOR MECHANISTIC-EMPRIRICAL PAVEMENT DESIGN

Linbing Wang, Ph.D., P.E.
Professor
Via Department of Civil and Environmental Engineering
Virginia Polytechnic Institute and State University
Blacksburg, Virginia

Yinning Zhang, Ph.D.
Graduate Research Assistant
Via Department of Civil and Environmental Engineering
Virginia Polytechnic Institute and State University
Blacksburg, Virginia

Brian K. Diefenderfer, Ph.D., P.E.
Associate Principal Research Scientist
Virginia Transportation Research Council
Charlottesville, Virginia

Benjamin F. Bowers, Ph.D.
Research Scientist
Virginia Transportation Research Council
Charlottesville, Virginia

INTRODUCTION

Moisture related problems have long been recognized as a primary cause of pavement failure. Water enters into the pavement structure through surface infiltration (in areas such as joints and cracks), from higher ground, rising ground water, capillary action and vapor movement[1]. The presence of water in a pavement structure is undesirable because it can adversely affect the performance of both asphalt and concrete pavements in many ways. In asphalt pavements, moisture can degrade the base, subbase and subgrade and strip asphalt coating from aggregate particles. In jointed concrete pavements, entrapped water can cause erosion of the subgrade and subbase creating voids beneath the concrete slab resulting in faulting and slab cracking.[2,3]

Moisture from various sources is usually prevented from entering the pavement structure or accumulating in the subgrade through surface and subsurface drainage approaches. It can be more cost effective and less risky to prevent water/moisture entry and accumulation using surface drainage than to remove water/moisture using subsurface drainage. To reduce the moisture induced premature deterioration for both asphalt and concrete pavements, over 30 states

have incorporated a permeable drainage layer as a part of their typical pavement structures. These may be constructed as daylighted layers or in conjunction with an edge drain system to prevent or minimize moisture accumulation.[4]

Pavements using drainage systems typically include three basic elements:

1) A permeable base layer (typically 2-4 inches thick) to provide for rapid removal of water that has entered the pavement structure;
2) A method of conveying the removed water away from the pavement structure (ranging from a sloped edge towards a drainage ditch to a pipe and collector system); and
3) A filter layer such as using a geotextile, graded aggregate layer or bound layer to prevent the migration of fines into the permeable base from the subgrade, subbase or shoulder.

To prevent material and structural failure in drainage layers, effective laboratory characterization is needed. The majority of the material failures in the drainage layer are related to the intrusion of fines from other layers into the drainage layer, causing clogging of drainage paths. To prevent fine intrusions, a dense-graded filter layer may be applied to separate the drainage layer from unbound layers. Additionally, the structural contribution of the drainage layer to a pavement structure is not considered in the 1993 AASHTO pavement design guide. Some states follow this approach and do not give the drainage layer a structural layer coefficient, although there are also states that do assign layer coefficients to drainage layers.

In AASHTO's Pavement ME design procedure, while each different layer can be evaluated individually, there is no procedure specifically developed to characterize the fundamental properties of the drainage layers, which are usually composed of high porosity asphalt/cement treated or granular materials with porosities ranging from 20% to 35%. With such high porosities, it is difficult to prepare laboratory specimens to evaluate the elastic modulus and the strength of these materials. Within this context, research is needed to develop new methods or modify existing methods to characterize the elastic modulus and strength of these materials at high porosity, to perform analysis of the stability and failure mechanisms of the drainage layer in the pavement structure, and to specify the required minimum porosity for effective drainage. The objectives and scope of this study are illustrated in following section.

In this study, basic information such as the typical materials, thickness, location, stiffness and permeability of the drainage layer were reviewed. This information was collected for typical drainage layer materials as identified by the state highway agencies from Idaho, Oklahoma, Wisconsin, and Virginia that participated in Transportation Pooled Fund Project 5(229).

PURPOSE AND SCOPE

The primary purpose of this study was to identify and perform tests to characterize typical pavement drainage layer materials for use with the mechanistic-empirical pavement

design procedures. While achieving the primary purpose, the study was also able to perform an analysis on the stability and potential failure mechanisms of the drainage layer in the pavement structure, and to develop recommendations for required minimum porosity for effective drainage.

Characterization testing was performed on materials collected from Idaho, Oklahoma, Wisconsin, and Virginia that were identified by the respective state highway agency that participated in Transportation Pooled Fund Project 5(229). The testing included determining the volumetric properties, permeability and stiffness of the asphalt treated permeable base specimens with three gradations and different air void contents through laboratory tests. For the cement treated permeable base materials, the volumetric properties, permeability and compressive strength were determined for specimens with different air void contents. Discrete Element Method (DEM) and Finite Element Method (FEM) were applied to predict the resilient modulus of unbound open-graded drainage layer materials and to investigate the structural contribution and location effect of the drainage layer to the pavement structure.

METHODS

Literature Review

A literature review was conducted by searching various databases related to transportation engineering such as the Transport Research International Documentation (TRID) bibliographic database, the catalog of Transportation Libraries (TLCat), and the Catalog of Worldwide Libraries (WorldCat).

Laboratory Testing

A series of laboratory tests were conducted to investigate the volumetric properties, permeability, and dynamic modulus of typical asphalt-treated permeable base (ATPB) materials and the compressive strength of the typical cement-treated permeable base (CTPB) materials from Idaho, Oklahoma, and Virginia. Unbound permeable base (UPB) material was collected from Wisconsin and tested for volumetrics, permeability, and resilient modulus. All tests were conducted in accordance with developed or modified AASHTO or ASTM standards or the local specification of each state. The ATPB materials from Oklahoma and Virginia were received as plant-mixed materials and specimens were fabricated in the laboratory. The ATPB material from Idaho and the Oklahoma CTPB material were received as loose aggregates (sampled by the agency); these materials were mixed in the laboratory where test specimens were prepared. Table 1 shows selected production details for ATPB and CTPB materials.

Table 1. Production Details for Asphalt- and Cement-Treated Drainage Layer Materials

Type	Property	Idaho	Oklahoma	Virginia
Asphalt Treated Permeable Base	Binder Performance Grade	64-28	64-22	70-22
	Asphalt Content, %	3.0	2.5	4.3
	Placement temperature, °F	280*	240	280
Cement Treated Permeable Base	Cement content, lbs/yd^3		270	
	Water-to-cement ratio		0.4	

*Materials from Idaho were produced in the laboratory, this temperature represents the laboratory mixing temperature

Gradation

The gradation of each set of materials received from the participating agencies was determined in accordance with AASHTO T27 *Sieve Analysis of Fine and Coarse Aggregates* and the results are shown in Table 2. The gradation of the unbound materials from Wisconsin was not measured as the material was pre-mixed by the sponsoring agency. Table 2 shows the recommended design ranges for the unbound material.

Table 2. As Received Gradation of Drainage Layer Materials

Sieve, in	Idaho	Oklahoma*	Virginia	Wisconsin
1 ½		100		
1.0		95	100	90-100
¾			92	
½	50	47	73	
3/8	35			45-65
No. 4	4	3		15-45
No. 8	1	2	4	
No.10				0-20
No.40				0-10
No. 200		1.4	1	0-5

*The same gradation was used for asphalt- and cement-treated materials from Oklahoma.

Specimen Preparation

Asphalt Treated Permeable Base

The ATPB plant-produced mixtures collected from Virginia and Oklahoma were used to compact specimens in the lab. Since the production of ATPB materials from Idaho were unavailable as plant-produced mixtures during the period of this study, the raw ingredients (aggregates, asphalt binder, and a typically-used additive (Superbond®)) were collected and then mixed in the laboratory. This mixture was prepared by mixing the desired aggregate gradation, asphalt binder, and additive in a bucket mixer (after all materials were heated to 280°F) in the laboratory as shown in Figure 1.

Figure 1. Asphalt Treated Permeable Base from Idaho Fabricated Using a Bucket Mixer.

All ATPB test specimens were fabricated using a gyratory compactor. Six-inch diameter specimens were compacted to a height of approximately 7 inches and with air void contents ranging from 18% to 32% in accordance with AASHTO T312 *Standard Method of Test for Preparing and Determining the Density of Hot-Mix Asphalt (HMA) Specimens by Means of the Superpave Gyratory Compactor* [5]. The prepared specimens were then cored and trimmed to 4 inches diameter and 6 inches height for further tests in accordance with AASHTO PP60 *Standard Practice for Preparation of Cylindrical Performance Test Specimens Using the Superpave Gyratory Compactor (SGC)*. To obtain specimens with different target air void contents, trial specimens were produced until the desired air voids were achieved. The materials were compacted at the placement temperatures shown in Table 1.

Cement Treated Permeable Base

Cement Treated Permeable Base (CTPB) materials from Oklahoma were used to investigate the mechanical properties using specimens having a 4 inch diameter and 8 inch height. The CTPB specimens were fabricated for compressive strength tests; the air void content of these specimens ranged from 27% to 35%. The received aggregates were remixed and then quartered prior to producing test specimens. Test specimens were produced in accordance with ASTM C192/C192M *Standard Practice for Making and Curing Concrete Test Specimens in the Laboratory* [6] using the cement content and water-to-cement ratio as shown in Table 1. Figure 2 shows the molded specimens after compaction.

Figure 2. Fabricated CTPB Specimens from Oklahoma.

After compaction, the specimens were stored at room temperature and moist cured. To simulate curing at construction, a fine spray of water was applied onto the surface of the specimens every two hours, for 16 hours. During storage, polypropylene sheets were applied to cover the specimens in their molds. Six specimens were each demolded for compressive strength testing at 7, 14, 21, and 28 days after fabrication.

Unbound Materials from Wisconsin

The unbound permeable base (UPB) material from Wisconsin was compacted at target densities and moisture content to reach different initial air void contents. The specimens were prepared and tested in accordance with AASHTO T307-99 *Standard Method of Test for Determining the Resilient Modulus of Soils and Aggregate Materials*.

Volumetric Properties

Aggregate Bulk Specific Gravity

The aggregate bulk specific gravity is a required parameter to predict the effective asphalt binder content, and to further predict the dynamic modulus of ATPB mixtures through empirical correlations. For the ATPB mixtures, the aggregate bulk specific gravity was determined in accordance with AASHTO T85, *Standard Method of Test for Specific Gravity and Absorption of Course Aggregate*.[7] The aggregate bulk specific gravity (G_{sb}) is calculated as the following:

$$G_{sb} = \frac{A}{B-C} \quad (1)$$

Where

A = mass of oven dry sample in air, g;
B = mass of saturated surface dry (SSD) sample in air, g; and
C = mass of SSD sample in water, g.

Mixture Theoretical Maximum Specific Gravity

The theoretical maximum specific gravities of the ATPB materials from Idaho, Oklahoma, and Virginia were determined in accordance with AASHTO T209 *Theoretical Maximum Specific Gravity and Density of Hot Mix Asphalt Paving Mixtures*.[8] Before the G_{mm} was determined, the mixture was heated in an oven for 2 hours to facilitate further handling. The aggregates were then separated carefully by hand to eliminate clumps of fine particles.

For each mixture the maximum theoretical specific gravity was determined twice and the average was used to calculate the air void content of different ATPB specimens. The maximum theoretical specific gravity (G_{mm}) of the Idaho, Oklahoma, and Virginia mixtures were found to be 2.525, 2.524, and 2.474, respectively and are calculated as follows:

$$G_{mm} = \frac{A}{A-C} \quad (2)$$

Where

A = mass of oven dry sample in air, g; and
C = mass of sample in water bath at 25°C, g.

To determine the air void contents of the CTPB specimens from Oklahoma, the theoretical maximum specific gravity of the CTPB mixture was determined through the same test method which had been applied on ATPB materials, except that the cement treated materials were not heated to separate the particles. The air void values of CTPB specimens were greater than that of the ATPB due to different compaction methods and gradations adopted.

Mixture Bulk Specific Gravity

Unlike traditional dense-graded asphalt mixtures, the materials used for drainage layers are more porous, leading to difficulties in determining the bulk specific gravity and air void content by traditional test methods. In this study, three approaches were considered – dimensional analysis, parafilm method and vacuum sealing method – for ATPB specimens. The vacuum sealing method was applied to quantify the air void contents of CTPB specimens.

Dimensional analysis

The bulk specific gravity (G_{mb}) by dimensional analysis is calculated by dividing the specimen volume (determined by measuring the diameter and height of each specimen) by the weight of dry specimen in air as follows:

$$G_{mb} = \frac{A}{\frac{1}{4}\pi d^2 h \rho_w} \quad (3)$$

Where

A = mass of oven dry sample in air, g; and
d = average diameter, cm;
h = average height, cm; and
ρ_w = density of water at 4°C.

The major source of error using this method lies in determining the volume of each specimen accurately, especially for large-air-void specimens.

Parafilm method and CoreLok vacuum sealing method

Calculating the G_{mb} when a saturated-surface dry (SSD) condition is required is also problematic for drainage materials as the internal water often drains out before the weight of saturated specimen can be determined. Additionally, when the surface is dried, internal water can be pulled to the surface from the large connected voids. These difficulties have been reported by other studies. [9, 10] As a result, the Parafim method and the CoreLok vacuum sealing method can be applied on open graded specimens to determine the G_{mb} and air void content as follows:

$$G_{mb} = \frac{A}{D - E - \left(\frac{D-A}{F}\right)} \quad (4)$$

Where

A = mass of oven dry sample in air, g; and
D = mass of parafilm-wrapped specimen in air, g;
E = mass of parafilm-wrapped specimen in water, g; and
F = specific gravity of the parafilm at 25±1℃ (0.922).

Figures 3a and 3b show an example of a specimen wrapped in parafilm and one that is vacuum sealed, respectively. It can be seen that the vacuumed sealing bag attached more tightly to the surfaces of the specimen compared with the Parafilm method.

Air Void Content

The air void content, also expressed by Voids in Total Mixture (VTM) can be calculated as follows:

$$VTM = \left(1 - \frac{G_{mb}}{G_{mm}}\right) x\ 100 \quad (5)$$

Figure 3a. Specimen Wrapped in Parafilm.

Figure 3b. Specimen Vacuum Sealed.

Permeability

It should be noted that currently there is no nationwide standard for determining the permeability of laboratory compacted specimens made with open graded or gap graded asphalt or cement mixtures. For this study, modifications to locally-used methods were employed. For the Virginia and Oklahoma ATPB materials, VTM-84 (Constant Head Test for Open Graded Drainage Layer Material) [11] and OMD L-44 (Flexible Wall Falling head Method to Determine Hydraulic Conductivity of Laboratory Compacted Specimens) [12], were used, respectively. To apply the falling head method to the ATPB specimens from Oklahoma, a customized inlet tube was used to obtain better results.

There is no local specification to determine the permeability of ATPB specimens from Idaho, therefore ASTM D5084 *Standard Test Methods for Measurement of Hydraulic Conductivity of Saturated Porous Materials Using a Flexible Wall Permeameter* was followed.[13] The constant head method was followed to test the CTPB materials from Oklahoma.

Constant Head Method (Virginia ATPB and Oklahoma CTPB)

The permeability of the Virginia ATPB and Oklahoma CTPB specimens was determined in accordance with VTM-84, a constant head method. Before applying a water head above each specimen, the specimen was wrapped tightly with a rubber membrane and was held by a cylindrical plastic mold which conformed tightly to the wrapped specimen. This prevented water flowing along the annular space between the mold and specimen during the permeability test and negatively affecting the results. Then, the specimen was placed on a suspension device which was submerged in a tray full of water. By keeping a constant water head above the specimen in the plastic mold and measuring the amount of water running out of the tray during a given time, the permeability (k) can be calculated as follows:

$$k = \frac{Q \times L}{H \times A \times t} \tag{6}$$

Where

Q = amount of water collected, (mm^3);
L = length of specimen, (mm);
H = head elevation, (mm);
A = cross sectional area of specimen, (mm^2); and
T = time, sec.

A schematic of the test setup for the constant head method as described in VTM-84 is shown in Figure 4. The water accumulated in the tray at the bottom of the frame is used to calculate the permeability.

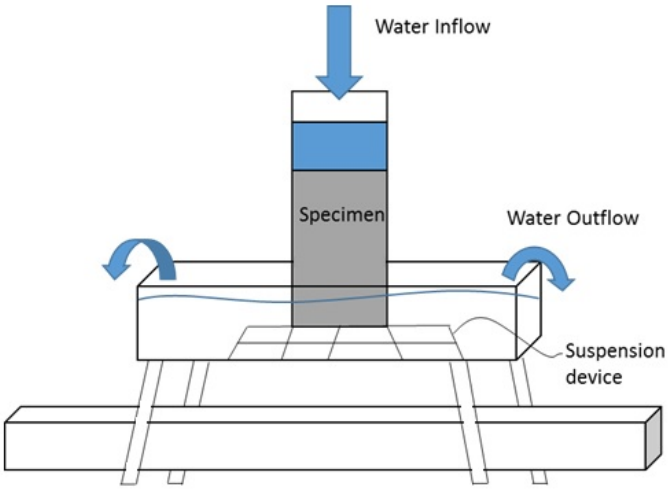

Figure 4. Schematic of Constant-Head Permeability Test.

Flexible Wall Falling Head Method (Oklahoma ATPB and Idaho ATPB)

The flexible wall falling head permeameter was used to determine the permeability of the Oklahoma and Idaho ATPB mixtures with different air void contents. According to previous studies [14], the degree of saturation may significantly influence the hydraulic conductivity of the asphalt concrete. To eliminate the impact of degree of saturation and focus on the influence of air void content on the permeability, all specimens were saturated before the testing. Testing was performed in accordance with AASHTO T283 *Standard Method of Test for Resistance of Compacted Asphalt Mixtures to Moisture-Induced Damage* to saturate the specimens by applying a vacuum of 20 inches of Hg for 10 minutes.[15] The specimens were then placed into a permeameter and a vacuum of 10 to 15 psi was applied to the specimen in the mold to get the rubber membrane to conform tightly to the surface of specimen, preventing water leaking through the annular space between specimen and membrane. By recording the time elapsed for the water head to change from the initial position to the final position, the permeability (k) can be calculated as follows:

$$k = \frac{aL}{At} ln\left(\frac{h1}{h2}\right) C \quad (7)$$

Where

a = inside cross-sectional area of the graduated cylinder, (mm^2);
L = length of specimen, (mm);
A = cross sectional area of specimen, (mm^2);
t = elapsed time between h1 and h2, sec;
h1 = initial head across the test specimen, (mm);
h2 = final head across the test specimen, (mm); and
C = temperature correction for viscosity of water.

Using the falling head method on the permeable materials for this study required the development of a customized permeameter having a larger inlet tube. Using a traditional permeameter with a 500 cm^3 water capacity was problematic in that it only took 2 to 3 seconds to empty the inlet tube making it difficult to accurately record the elapsed time. To increase the elapsed time, a customized permeameter with a 2000 cm^3 capacity was adopted as shown in Figure 5. For each specimen, the permeability was taken as the average of two trials.

Figure 5. Customized Permeameter to Determine Permeability of ATPB Specimens.

Dynamic Modulus for ATPB Specimens

The dynamic modulus (the absolute value of the complex modulus) is defined as the ratio of the peak stress (σ_0) and the peak strain (ε_0) under certain loading frequency and temperature combinations for asphalt bound materials. The dynamic modulus can be calculated as follows:

$$|E^*| = \frac{\sigma_0}{\varepsilon_0} \tag{8}$$

For mechanistic-empirical pavement design approaches using asphalt materials, the dynamic modulus is the primary input parameter. However, since ATPB materials are not as stiff as typical dense-graded asphalt mixtures, strictly following the guidelines in AASHTO T342-11 *Standard Method of Test for Determining Dynamic Modulus of Hot Mix Asphalt (HMA)* [15], may not be applicable on the ATPB specimens. AASHTO T342 recommends testing at temperatures of -10, 4.4, 21.1, 37.8, and 54.4°C and at test frequencies of 25, 10, 5, 1, 0.5, and

0.1Hz. This study sought to develop a customized test method. All dynamic modulus testing was conducted on an Interlaken Compact Soil & Asphalt Test System controlled by Unitest software.

Generally, the reasons for modifying the conventional dynamic modulus test to facilitate its application on ATPB materials include: 1) Since the ATPB material is expected to be subjected to a lesser high temperature, given its location within a pavement structure, the high test temperatures recommended for asphalt mixtures possibly violates the linear viscoelastic assumptions when using ATPB specimens; an example when this assumption is violated on an ATPB specimen is shown in Figure 6. 2) Conventional stress levels are likely too large for ATPB to keep the strains within the recommended range of 50-150 με. 3) There is no experience in the literature on the conditioning time of any potential modified testing temperatures on ATPB specimens.

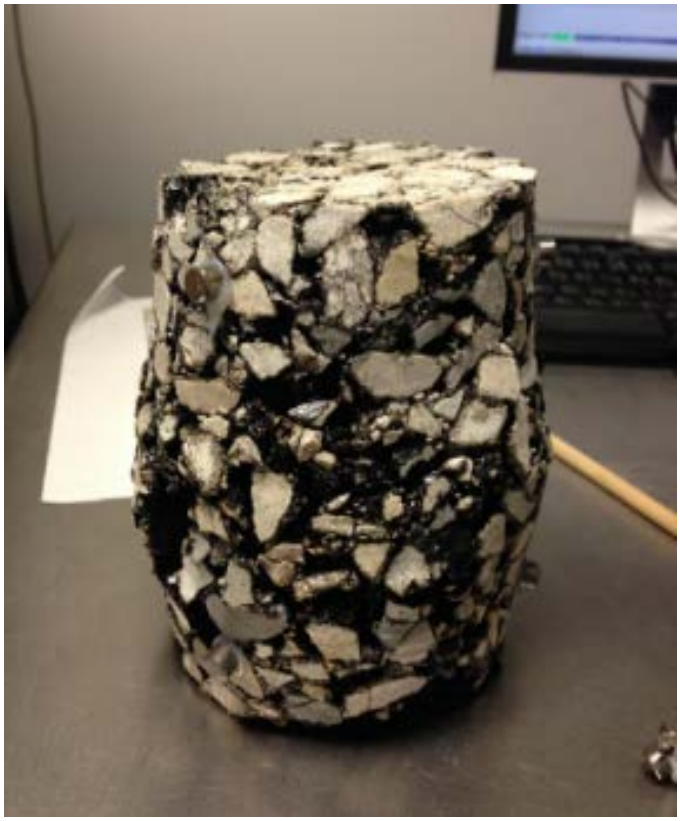

Figure 6. Plastically Deformed ATPB Specimen During Dynamic Modulus Testing at High Stress Levels and High Temperatures.

Determining Appropriate Stress Levels

As shown in Figure 6, traditionally-used stress levels can be problematic when testing ATPB specimens. To determine appropriate stress levels, 30 ATPB specimens were fabricated with different air void contents and tested by observing the strains under different stress levels. At high void contents, high test temperatures, and low frequencies, it was difficult to keep the

strains less than 150 με. However, it was found that the stress level could only be reduced so far and still collect quality data. Given this limitation, it was necessary to increase the tolerable strain level for this was increased to 200 με. The frequencies, stress magnitudes, and number of cycles applied during the dynamic modulus testing in this study are listed in Table 3.

Table 3. Frequency, Stress Level, and Cycles Applied at Different Temperatures for Dynamic Modulus Testing

Temperature ℃ (℉)	Frequency	Stress Level (kPa)	Cycles	Recommended Stress Level, AASHTO T342-11 (kPa)
4.4 (40)	25	500	200	700-1400
	10	500	200	
	5	400	100	
	1	400	20	
	0.5	300	15	
	0.1	300	15	
12.7(54.9)	25	300	200	N/A
	10	300	200	
	5	250	100	
	1	250	20	
	0.5	200	15	
	0.1	200	15	
	10	50	200	
21.1 (70)	25	200	200	350-700
	10	200	200	
	5	150	100	
	1	150	20	
	0.5	100	15	
	0.1	100	15	
29.4(84.9)	25	100	200	N/A
	10	100	200	
	5	75	100	
	1	75	20	
	0.5	50	15	
	0.1	50	15	
37.8 (100)	25	50	200	140-250
	10	50	200	
	5	30	100	
	1	30	20	
	0.5	15	15	
	0.1	15	15	

Determining Appropriate Test Temperatures

In addition to modifying the stress level, the test temperatures were also modified. This was done for two reasons. First, unlike the surface courses, the drainage layer is typically located deeper within the pavement structure and so is not subjected to higher temperatures. Previous studies showed that the temperatures at depths typical for drainage layers are approximately 30°C to 35°C in July in Los Angles [16] and approximately 25°C in Virginia.[17] Second, it was thought that the drainage layer could become unstable at test temperatures of

54°C and violate the assumption of linear viscoelastic behavior. This is evidenced by the low stress levels applied at 0.5 and 0.1 Hz and at the 37.8°C test temperature to keep the strain less than 200 με as shown in Table 3.

To further investigate the potential temperature distribution inside a drainage layer in the three states where ATPB materials were sampled, the climate data of Lynchburg, VA, Oklahoma City, OK, and Boise, ID were used in the Enhanced Integrated Climate Model (EICM), which was used to predict the pavement temperature at typical depths. According to the calculated temperature distribution, the highest temperatures inside the drainage layer occur in July, and the means are all below 34℃ in the three states, as shown in Figure 7. Figure 8 shows the quintile temperatures associated with 10%, 30%, 50%, 70% and 90% probability for the month of July. Figure 8 indicates that there is a 70% probability that the temperatures inside the drainage layer are below approximately 38℃.

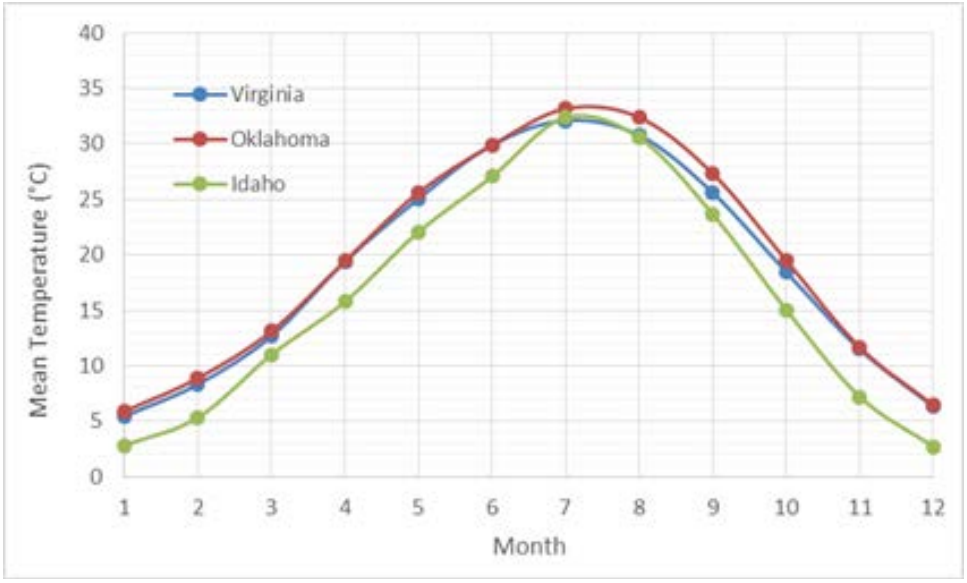

Figure 7. Mean Pavement Temperature at Typical ATPB Depths for Virginia, Oklahoma, and Idaho Calculated by Enhanced Integrated Climatic Model.

From the results of previous studies and the temperatures predicted by EICM in this study, the highest and lowest recommended temperatures in AASHTO T342-11 (-10 and 54.4°C) were not used for dynamic modulus testing. However, two additional temperatures, 12.7°C and 29.4°C, were added to the temperatures recommended by AASHTO T342 (4.4℃, 21.1℃ and 37.8℃).

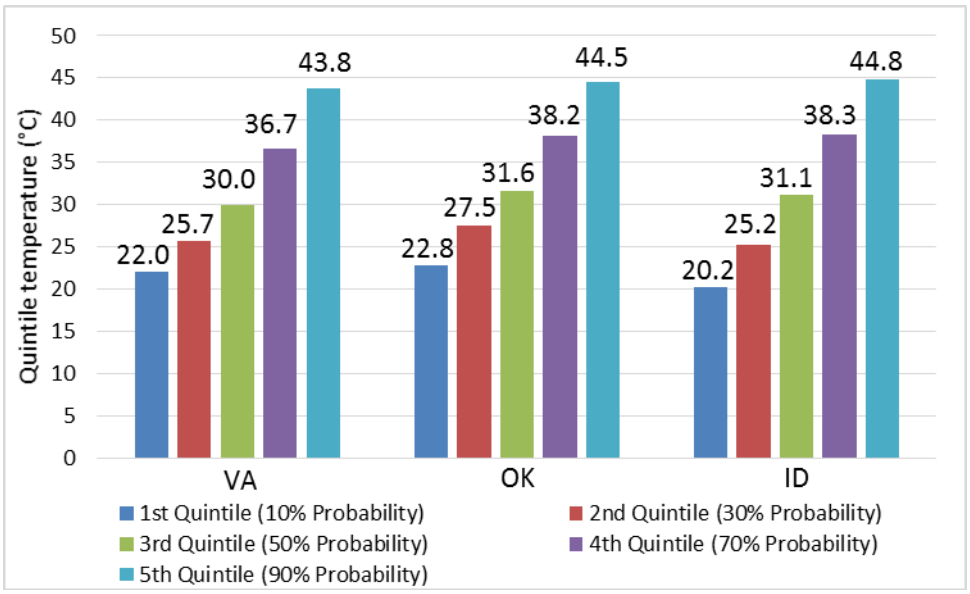

Figure 8. Quintile Pavement Temperatures in July at Typical ATPB Depths for Virginia, Oklahoma, and Idaho Calculated by Enhanced Integrated Climatic Model.

Determining Conditioning Time

The conditioning time for specimens to reach the desired test temperatures are recommended by AASHTO T342-11. However, these recommendations are for dense-graded materials and not open-graded ATPB materials. To determine appropriate conditioning times, a thermometer was embedded in a trial specimen placed in a temperature chamber to monitor the time required to reach test temperatures. Figure 9 shows an example of the specimen temperature versus conditioning time when transitioning from room temperature to 37.8°C. The designations *1st measurement* and *2nd measurement* in the figure refer to replicate specimens.

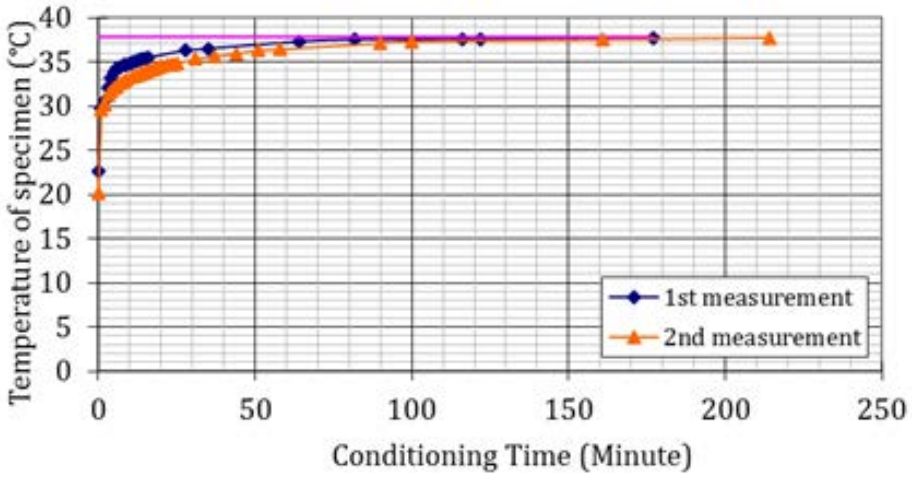

Figure 9. Conditioning Time for an ATPB Specimen From Room Temperature to 37.8°C.

From this testing, the required conditioning times to reach the desired temperatures were found and are shown in Table 4. Both the required time to condition the specimens from room temperature and from the previous test temperature are provided. All the conditioning times were determined based on the temperature monitoring results to ensure equilibrium is reached throughout the specimen. For other environmental chambers, the conditioning time could vary slightly. However, the conditioning time for ATPB materials was generally found to be shorter than for dense-graded asphalt mixtures, likely due to the higher air void content of the ATPB specimens.

Table 4. Time to Condition ATPB Specimens

Temperature °C (°F)	**Time to condition the specimens from room temperature**	**Time to condition the specimens from previous test temperature**
4.4 (40)	Overnight	
12.7(54.9)	3 hours	2 hours
21.1 (70)	1 hour	1.5 hours
29.4(84.9)	1.5 hours	1 hour
37.8 (100)	2 hours	1 hour

Resilient Modulus Test

Resilient modulus is a fundamental material mechanical property widely adopted for describing unbound granular materials. Cyclic axial loadings at different magnitudes are rapidly applied on the cylindrical sample in a pressure chamber to determine the resilient modulus. Based on particle size and plastic properties of fines, the unbound materials from Wisconsin were classified as Type 1 material according to the test procedures AASHTO T 307-99 *Standard Method of Test for Determining the Resilient Modulus of Soils and Aggregate Materials*. The samples were placed into molds that had a 6-inch diameter and a 12-inch height for the resilient modulus test. A total of 1000 repetitions of conditioning loads and 15 different load sequences with increasing confining pressure and varying cyclic load were applied. The conditioning load and cyclic load were all Haversine-shaped pulses of 0.1 second followed by 0.9-second rest period.

In each load sequence with fixed target confinement and cyclic loading, the resilient modulus was calculated at each of the last five cycles using Equation 9, and the average was used as the dynamic modulus for this sequence.

$$M_R = \frac{\sigma_d}{\varepsilon_r} \tag{9}$$

where

M_R is the resilient modulus;
σ_d is the repeated deviator stress; and
ϵ_r is the recoverable elastic strain in axial direction.

Figure 10 shows the apparatus used in the resilient modulus test in this study for the unbound drainage layer materials from Wisconsin. Figure 11 shows the sample with 20% air void content during the resilient modulus test under 15 psi confining pressure.

Figure 10. Resilient modulus test apparatus.

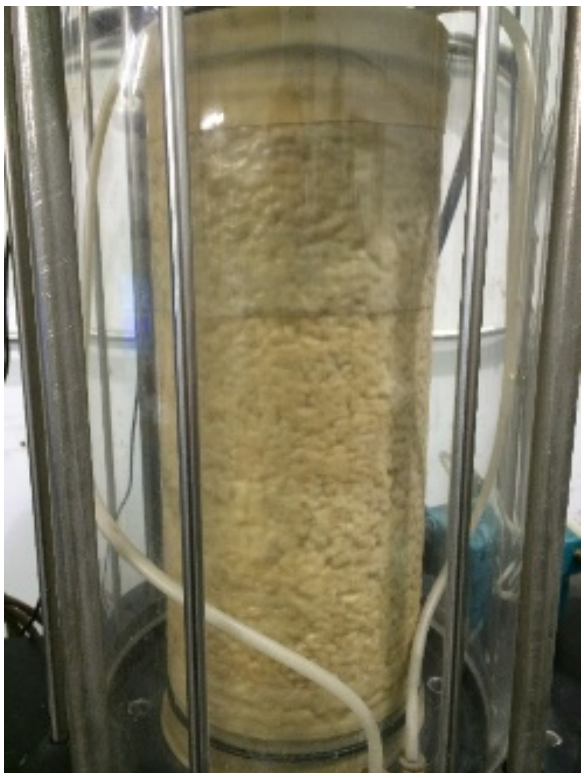

Figure 11. Sample with 20% air void content under 15 psi confining pressure.

Compressive Strength Testing for CTPB Specimens

At 7, 14, 21, and 28 days after fabrication, the compressive strength of CTPB specimens was determined in accordance with ASTM C192/C192M *Standard Practice for Making and Curing Concrete Test Specimens in the Laboratory*. Specimens were first capped with bonded gypsum to level the ends and provide a uniform distribution of loading. They were next mounted under the load cell and loaded to failure. The maximum force applied was recorded and the compressive strength of each specimen was calculated by dividing the maximum force by the cross sectional area of the specimen. The capped specimen and the setup for the compressive strength test are shown in Figures 12 and 13.

Figure 12. Capped CTPB Specimen.

Figure 13. Capped CTPB Specimen Loaded for Compressive Strength Testing.

RESULTS AND DISCUSSION

Literature review

Drainage Layer Types

In addition to serving the important function of removing water from a pavement structure, the drainage layer also works as a load bearing layer. The selection of the optimal material for a drainage layer is a tradeoff between permeability and mechanical properties such as stability, stiffness and strength. Omitting the fines in a gradation can increase the permeability but will negatively affect the stability and other mechanical properties of the drainage layer. Therefore, to balance between the permeability requirement and desired mechanical properties, part of the fines in a dense gradation can be removed or the material can be stabilized. This represents the two types of typical drainage layer materials: unstabilized and stabilized. An unstabilized drainage layer requires some fine aggregates to improve the interlock between the particles, ultimately providing stability. The stabilized drainage layer does not require fines for stability, although fines may be used, but rather relies on a stabilizer to provide cementing between particles. The typical stabilizing materials include asphalt binder and hydraulic cement.

Gradation

The recommended gradation usually differs for the unstabilized and the stabilized drainage layers. A limited amount of fines are usually allowed in an unstabilized drainage layer to keep stability under construction and traffic loading. Generally, the gradation used is for the sake of stability during construction operation. The gradation of an unstabilized drainage layer is often determined in accordance with two criteria: (1) sufficient permeability capacity and (2) enough stability and strength. The Norwegian Road Research Laboratory found that the percent passing No.200 sieve should not exceed 9% for a gravel base drainage layer to achieve acceptable permeability capacity and shear strength.[5] An Illinois research study suggested that sieves smaller than 2mm (No.10) should be minimized for the permeable base material. The U.S. Army Corps of Engineers recommended a Rapid Draining Material and an Open Graded Material for the drainage layer in an airfield pavement.[18] The American Concrete Pavement Association (ACPA) suggested an increase in intermediate aggregates to the American Association of State Highway Transportation Officials (AASHTO) No.57 or No.67 gradation for the unstabilized drainage layer.[19] Today, many states have their own requirements on the gradation of unstabilized drainage layer materials in the local specifications.

With respect to stabilized drainage layers, several state agencies use the AASHTO No. 57 gradation or a variation thereof for their stabilized permeable bases. The Wisconsin Department of Transportation (DOT) has reported success with using the AASHTO No. 67 gradation in stabilized bases.[1] Florida DOT has reported that their typical ATPB was a No.57 or No.67 according to a statewide evaluation.[20] In some states a combination of No. 57 and No. 67gradations is adopted for better performance. The amount of material passing the No.200 sieve is often limited to 0 to 2% to reduce the amount of fines by some states.[1] Many studies have been focused on improving the gradations of stabilized aggregate. Virginia DOT utilized a

50-50 blend of No.68 and No.8 aggregate with a thick asphalt film in a flexible pavement and received good results in both constructability and durability.[21]

Stabilizer Content

It is reported that many highway agencies utilize lightly stabilized ATPB materials with an asphalt content in the range of 2 to 3% and a cement content of 100-280 lbs/yd^3 for CTPB drainage layers.[4,19, 22]

Drainage Layer Thickness

To ensure the structural performance as well as the hydraulic capacity of the pavement, the thickness of each layer is first determined by satisfying the structural requirement to support traffic loading. The drainage capacity is next checked to see whether the thickness is appropriate from a drainage perspective.[2]

For ATPB, the Federal Highway Administration (FHWA) has recommended the thickness to be 4 to 6 inches for drainage blankets early in 1972 [23]. Mathis suggested 4 inches of ATPB as a drainage layer.[10] Forsyth indicated the range of ATPB used is from 3 to 6 inches and the most common thickness of ATPB is 4 inches.[24] California specifies 3 inches of ATPB for a drainage layer and Oregon uses 3 to 4 inches ATPB in several designs.[25] According to an evaluation of asphalt treated permeable base conducted by the Florida DOT, the thickness of the ATPB layers in several concrete pavements throughout the state are typically 4 to 5 inches.[7] For CTPB, the typical thickness ranges from 3 to 6 inches, with the most common value being 4 inches. The thickness of untreated permeable base used in Oregon typically ranges from 6 to 15 inches [25].

Drainage Layer Locations

To effectively remove the water which has infiltrated into the pavement, the drainage layer should be located at a depth to allow for drainage within the required time limit. It is recommended that, for the highest-class highways, the time for draining 50% of the free water be within 1 hour, and for most interstate highways the limit is 2 hours.[1] As a result, drainage layer should be located at a depth where the drainage pathway is short enough for effective draining according to different pavement classes. At the same time, it should not be placed too near the surface to ensure stability. Typically the drainage layer is located below or as a part of the base course.[14]

The typical location of drainage layers in pavement structures are shown in Figures 14 and 15.[14] Figure 14 shows the base working as a drainage layer. Therefore the drainage layer should satisfy both the permeability and the strength requirements. The disadvantages of a drainage layer within the pavement base includes the potential for inadequate stability and inability for draining water in the subbase and lower structure. Figure 15 shows the drainage layer below subbase or as part of subbase. The disadvantage of a drainage layer in this location is that the length of the water pathway from surface infiltration is relatively longer therefore the

pavement may take more time to drain. The permeability of the base and subbase materials should be greater than the infiltration rate to eliminate trapping water within the drainage layer.

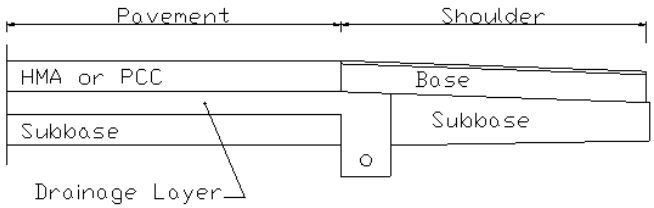

Figure 14. Example of Including a Drainage Layer as Part of the Pavement Base. [13]

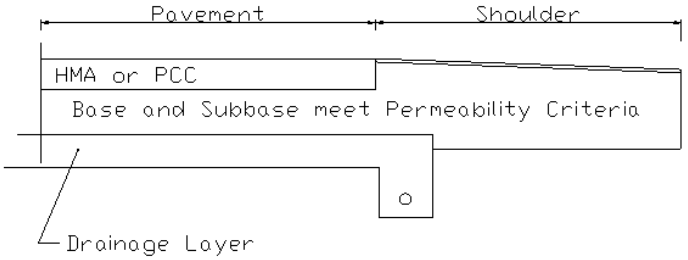

Figure 15. Example of Including a Drainage Layer as Part of the Pavement Subbase. [13]

Strength of Drainage Layers

The resilient modulus of ATPB materials with very high air void contents (ranging from 34.2% to 35.7%) was investigated by the University of California, Berkley and Caltrans.[26] The resilient modulus was obtained under different stress levels with the sum of the principal stresses of 200 kPa, 500 kPa and 1000 kPa through laboratory testing.[26] The as-compacted resilient modulus of ATPB used for the pavement design based on the Caltrans method and elastic layer theory is 1172 MPa.[27] The ranges of the resilient moduli of the ATPB mixtures are from a minimum of 689 MPa to a maximum of 1034 MPa, and the modulus of 1034 MPa for the ATPB was used to model the pavement fatigue life.[14] Loulizi et al. assigned the modulus of 1034 MPa for the permeable layer in their study to calculate the vertical stress responses within the pavement.[16] In another study, the resilient modulus was recommended to be 762 MPa for an ATPB according to a Vermont Department of Transportation pavement design committee.[28]

Compared with conventional dense-graded asphalt mixtures, the modulus of ATPB is much lower. The stiffness of ATPB materials was reported to be on the order of 1000 MPa in the dry state and approximately half this value in a wet condition [26]. The stiffness of conventional asphalt mixtures can be 5.5 to 7 times greater than the stiffness of ATPB even in dry state.[26] Based on the back-calculated effective pavement thickness, it was found that a pavement incorporating a permeable asphalt treated aggregate base would be less stiff than a pavement with a dense-graded asphalt base in SPS-1 experiments conducted as part of the Long-Term Pavement Program (LTPP).[29]

For CTPB materials, the typical compressive strength of CTPB materials ranges from approximately 3.5 MPa to 7 MPa, at ages of 7-days or 14-days based on both laboratory and field tests.[30] Therefore, the drainage layer can be considered as a weak load bearing layer in the pavement structure and its strength should be checked and incorporated into the pavement structural analysis for further study.

Stress State Within Drainage Layers

The stress within the drainage layer varies with different pavement structures and temperatures. The practical stress levels inside the drainage layers are typically lower than that in the surface layers. Loulizi et al. conducted field measurements of the compressive vertical stress under the asphalt surface and above a permeable layer. The study showed that the vertical stresses under a 9.5 mm nominal maximum aggregate size (NMAS) asphalt mixture vary with the temperature and range from less than 50 kPa to more than 200 kPa when the structure is subjected to an 80-psi tire pressure.[31] Al-Qadi et al. measured the vertical stress under an asphalt mixture for a single load of 25.8 kN on a pavement with 3-in asphalt stabilized open graded drainage layer locating below the base course. The vertical stress varies with temperature and ranges from less than 50 kPa to more than 250 kPa from 0℃ to 40℃. The vertical stress at 20℃ is about 80 kPa, which shows consistency with typical former results.[32]

Permeability Tests on Asphalt Mixtures

There are generally two testing methods to determine the hydraulic conductivity of asphalt mixtures in the laboratory; these are the *constant head method* and the *falling head method*. The specification ASTM D5084 *Standard Test Methods for Measurement of Hydraulic Conductivity of Saturated Porous Materials Using a Flexible Wall Permeameter* is the standard test protocol of the falling head method. According to this method, materials with hydraulic conductivities greater than 1×10^{-5} m/s may be determined in accordance with Test Method D2434 *Standard Test Method for Permeability of Granular Soils (Constant Head)*, which is the constant head method. However, the ASTM D2434 may not be suitable for laboratory-compacted ATPB and CTPB specimens, or road cores, since it requires compacting specimens in the permeability testing container right before the test is conducted. Many states have specific local testing methods to determine the permeability of asphalt mixture specimens in the laboratory. Virginia validates the constant head method to determine the hydraulic conductivity of asphalt mixture with high permeability, as described in VTM-84. Oklahoma applies a flexible wall permeameter for laboratory permeability testing of regular asphalt mixtures as described in Oklahoma testing method OHD L-44. However, since ATPB's are much more porous than dense-graded asphalt mixtures, the inlet cylinder tube should be larger to ensure the time during the falling water head is not too short and is easy to be recorded. To investigate the permeability of unbound aggregate base Khoury et al. used a device with a longer inlet tube and a larger diameter than that provided by the typical flexible wall permeameter[33].

Stiffness Tests on Asphalt Mixtures

As a viscoelastic material, the relationship between stress and strain of asphalt mixtures is described by the complex dynamic modulus E*. The complex dynamic modulus relates the peak stress to peak strain for the viscoelastic materials subject to continuous sinusoidal loading. The dynamic modulus is defined as the absolute value of the complex modulus. To determine the dynamic modulus of asphalt mixtures in a laboratory, typically five different test temperatures and six different loading frequencies are applied, to investigate the time and temperature dependency. The specification AASHTO T342-11 *Standard Method of Test for Determining Dynamic Modulus of Hot-Mix Asphalt Concrete Mixtures* is the current test protocol for determining the dynamic modulus of dense-graded asphalt mixtures.[15] There are currently no specific test protocols designed for ATPB mixtures. Under some circumstances, reduced test temperatures and loading frequencies can also be used to describe the dynamic modulus of asphalt mixtures and to construct the master curves. The dynamic modulus at least at three temperatures and three frequencies determined in laboratory testing are allowed in Mechanical-Empirical pavement level 1 design. In order to construct master curve for the asphalt mixture, seven frequencies are required.[34]

Drainage Layer Failures and Problems

During the service life of a drainage layer, the materials may experience failures due to the combined effects of traffic loading and the environment. The California Department of Transportation (Caltrans) and the Indiana Department of Transportation (INDOT) both reported the material failures including fines injection from the beneath base course into an ATPB, and the stripping of asphalt coatings within the drainage layer. In addition to these material failures, the structural capacity of the stabilized permeable base may deteriorate when exposed to moisture or poor environmental conditions. Once the drainage layer loses its structural capacity, the pavement structure will be affected and damage can be caused. Illinois monitored the effectiveness of drainage layer in nine pavements during late 1980's and early 1990's, finding two of them deteriorated quickly in forms of superficial distresses, severe lane to shoulder settlement and high deflections.[35]

Material Collection from Participating States

The four participating state agencies (Idaho, Oklahoma, Virginia, and Wisconsin) provided information about the composition and use of drainage layers in pavements within their states. In addition, the agencies collected and shipped samples of these drainage layer materials for laboratory testing. All the materials collected and tested are representative of the typical drainage layer materials adopted by the participating states. All agencies, except for Wisconsin, typically use one or more treated open-graded material as a drainage course; Wisconsin typically employs an unbound aggregate layer.

Idaho

An asphalt-treated material is typically used for drainage layers by the Idaho Department of Transportation (ITD). The typical gradation requirements are shown in Table 5. The asphalt

binder used is a PG 64-28 and consists of approximately 3% by weight of aggregate. All the ATPB materials used for a drainage layer in Idaho are to use an approved anti-strip additive at minimum rate of 0.5% by weight of the asphalt binder.[36] The minimum air void content of the ATPB used in Idaho is 20%.

Table 5. Specified Gradation for Idaho Transportation Department ATPB

Sieve Size, in (mm)	Percent Passing (by Weight)
1.0 (25.0)	100
¾ (18.75)	90-100
½ (12.5)	35-65
3/8 (9.5)	20-45
No. 4 (4.75)	0-10
No. 8 (2.36)	0-5
No. 200 (.075)	0-2

Oklahoma

The Oklahoma Department of Transportation (ODOT) utilizes both an asphalt- and cement-treated drainage layers; gradation requirements are shown in Table 6.[37]

Table 6. Specified Gradation for Oklahoma DOT Drainage Mixtures

Sieve Size, in (mm)	Asphalt Treated Permeable Base	Cement Treated Permeable Base
	Percent Passing (by Weight)	
1 1/2 (37.5)	100	100
1.0 (25.0)	95-100	95-100
½ (12.5)	25-60	25-60
No. 4 (4.75)	0-10	0-10
No. 8 (2.36)	0-5	0-5
No. 200 (.075)	0-3	0-2

A minimum cement content of 240 lbs/yd^3 (142 kg/m^3) and a water-to-cement ratio of less than or equal to 0.45 is specified for the OGHCCB. A PG 64-22 asphalt binder is specified for the OGBB with an approved anti-stripping agent at the rate of 5 gal per 1,000 gal of binder to improve water-resistance performance.

Virginia

The specification for Virginia Department of Transportation (VDOT) ATPB is shown in Table 7. A PG70-22 asphalt binder is specified with an asphalt content of 4.3% ± 0.3%; the mixture to be placed at a temperature between 250°F to 280°F.[38]

Table 7. Specified Gradation for Virginia DOT ATPB

Sieve Size, in (mm)	Percent passing by weight (%)	
	Min.	Max
1.0 (25.0)	100	100
3/4 (19.0)	88	100
½ (12.5)	70	90
No. 8 (2.36)	0	15
No. 200 (0.075)	0.5	4.5
Asphalt Content 4.3 ± 0.3%		

Wisconsin

The Wisconsin Department of Transportation (WisDOT) typically specifies an UPB having a gradation as shown in Table 8. The UPB can be derived crushed aggregate, crushed gravel, or crushed concrete.[39]

Table 8. Specified Gradation for Wisconsin DOT UPB

Sieve Size, in (mm)	Percent Passing (by Weight)
1.0 (25.0)	90-100
3/8 (9.5)	45-65
No. 4 (4.75)	15-45
No. 10 (2.54)	0-20
No. 40 (0.635)	0-10
No. 200 (.075)	0-5

Laboratory Test Results

Based on the series of laboratory tests performed on about 200 specimens including asphalt and cement treated open graded drainage layer materials from Virginia, Oklahoma and Idaho, data analysis has been conducted and the results have been presented in this section.

Volumetric Properties

The volumetric properties are basic material properties influencing both the permeability and the mechanical performance. Therefore, the selection of proper test method to determine the volumetric properties of the treated open-graded drainage layer materials with large air void content is the prerequisite for further study.

Bulk Specific Gravity of Aggregate and Theoretical Maximum Specific Gravity of Mixture

The bulk specific gravity of the aggregate (G_{sb}) was determined in accordance with AASHTO T85 *Standard Method of Test for Specific Gravity and Absorption of Coarse Aggregate*; the results are shown in Table 9. The maximum specific gravity of the ATPB mixtures was determined following AASHTO T209 *Theoretical Maximum Specific Gravity and Density of Bituminous Paving Mixtures*; the results are shown in Table 9.

Table 9. Volumetric Properties for Permeable Drainage Mixtures

Property	Virginia	Oklahoma	Idaho
G_{sb}	2.578	2.680	2.569
G_{mm}	2.474	2.524 / 2.687*	2.525

*2.524 = G_{mm} for ATPB, 2.687 = G_{mm} for CTPB

Air Void Content

The dimensional method, parafilm method and vacuum sealing method (CoreLok) were performed on ATPB materials from Virginia and Oklahoma to determine the most suitable method to calculate the bulk specific gravity and hence the air void content of the mixture. A comparative and statistical approach was taken in effort to identify which method may produce the least variability between mixtures. This comparative and statistical effort is outlined in Appendix A. Following this analysis, the selected methods were used for the remaining mixtures from Idaho and Oklahoma.

As a result of the comparative and statistical analysis, it was found that when the VTM is greater than 24%, the difference between parafilm method and vacuum sealing method becomes significant. Therefore, in laboratory testing, the dimensional method can be used for specimens of less than 21% VTM and Parafilm method is good to test specimens of less than 24% VTM, for the sake of cost efficiency. The vacuum sealing method should be applied for specimens of VTM larger than 24%. To determine which method should be applied first, an estimation of the air void content by the dimensional method can be used. However, in practice, there may be large variations between the real and target air void content, or the batches of specimens have wide ranges of air void contents. In this case, it is more important to conform to a consistent test method, and the vacuum sealing method is preferable.

Permeability versus Air Void Content

Following the local and national modified or standard permeability test protocols, correlations between the permeability and air void content were found. The air void content of the Virginia ATPB specimens were obtained by Parafilm method rather than the vacuum sealing method due to the equipment problems encountered. The air void content of the Oklahoma and Idaho ATPB specimens were obtained by the vacuum sealing method. The permeability of the Virginia specimens was found by constant head method in accordance with Virginia Test Method (VTM) 84. Figure 16 shows that the permeability has a more rapid increase as the air void content increases when compared to the mixtures shown in Figures 17 and 18 which were tested using the falling head method. As a check, the constant head method was also used for the ATPB specimens from Oklahoma and it was found that the constant head method typically yields larger permeability results than the falling head method. This indicates that differences in the output from the different test methods exist and should be considered when the permeability obtained from different methods are used for comparison. The permeability of the Idaho ATPB was obtained using the flexible wall falling head method. When compared with the Virginia and Oklahoma ATPB materials, the permeability of the Idaho ATPB material changes little with air void content.

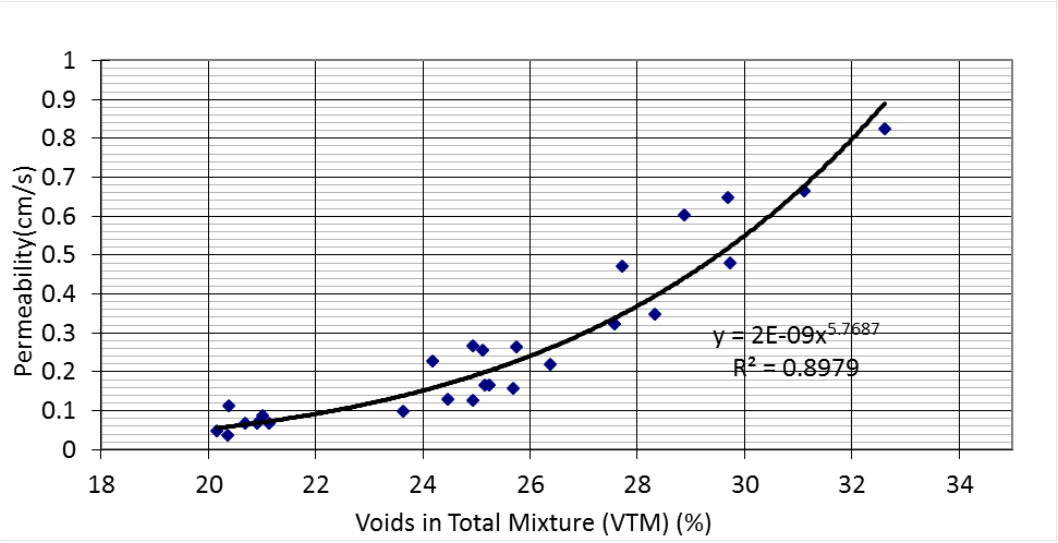

Figure 16. The Relationship between the Air Void Content (VTM) and Permeability for Virginia ATPB Specimens.

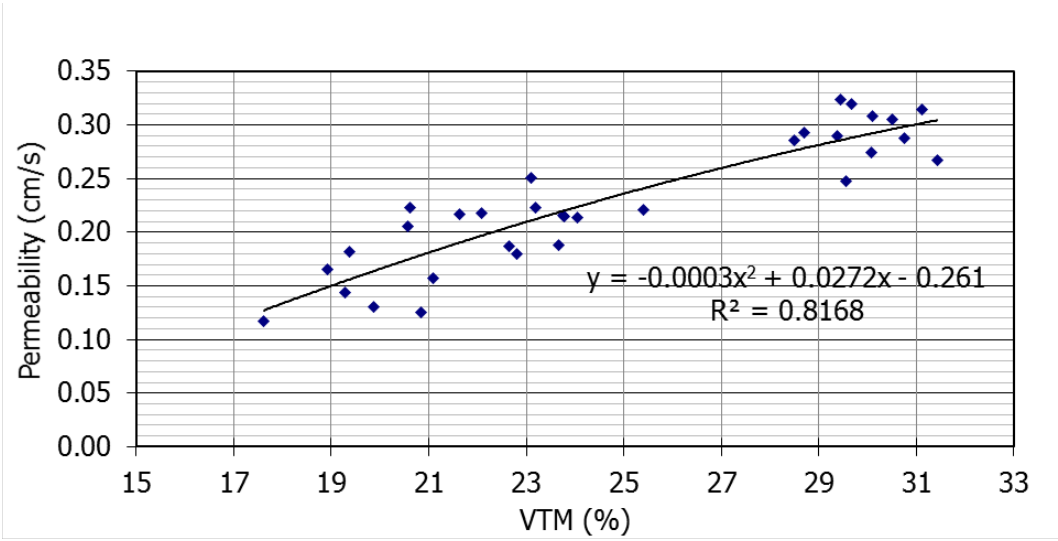

Figure 17. The Relationship between the Air Void Content (VTM) and Permeability for Oklahoma ATPB Specimens.

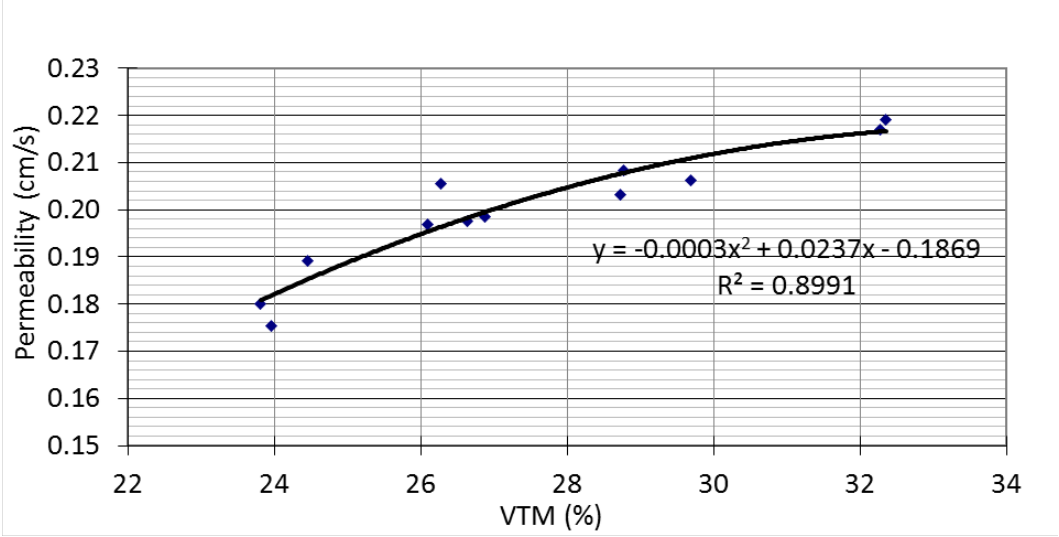

Figure 18. The Relationship between the Air Void Content (VTM) and Permeability for Idaho ATPB Specimens.

From Figures 16-18, regression analysis was used to describe the relationship between air void content (%) and permeability (cm/s). These relationships, along with their respective coefficient of determination (R^2), for the ATPB materials from Virginia, Oklahoma, and Idaho are given in Equations 10-12, respectively:

$$Permeability_{Virginia} = 2 \times 10^{-9} VTM^{5.7687} \quad R^2=0.8979 \tag{10}$$

$$Permeability_{Oklahoma} = -0.0003 \times VTM^2 + 0.0272 \times VTM - 0.261 \quad R^2=0.8168 \tag{11}$$

$$Permeability_{Idaho} = -0.003 \times VTM^2 + 0.0237 \times VTM - 0.1869 \quad R^2=0.8991 \tag{12}$$

Since there is no standard test method to determine the permeability of cement treated open graded materials, the constant head method was used for the CTPB materials from Oklahoma. The relationship between air void content and permeability is shown in Figure 19.

The permeability of CTPB specimens was found to be much higher than that for the ATPB specimens even when both materials were tested using the constant head method. This is likely attributable to larger void spaces between the specimen and the permeameter wall. ATPB specimens were fabricated by coring specimens prepared in the gyratory compactor. As such, the sides of the cylindrical specimens were relatively smooth. However, the CTPB specimens were fabricated by placing the materials in a mold having the same diameter as the permeameter. This resulted in larger void spaces along the sides of the cylindrical CTPB specimens.

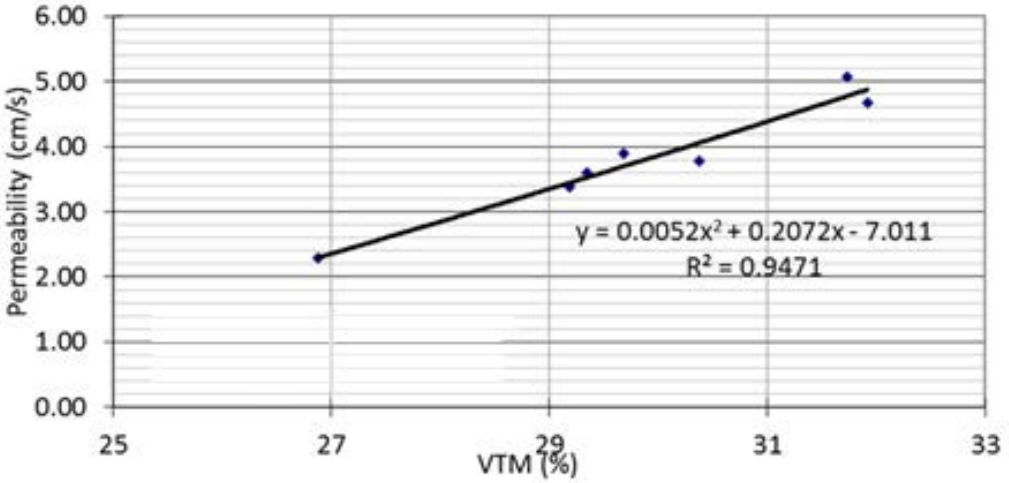

Figure 19. The Relationship between Air Void Content (VTM) and Permeability for Oklahoma CTPB Specimens.

From Figure 19, regression analysis was used to describing the relationship between air void content (%) and permeability (cm/s). This relationship, along with the respective coefficient of determination (R^2), for the CTPB materials from Oklahoma is given in Equation 13:

$$Permeability_{Oklahoma} = -0.0052 \times VTM^2 + 0.0207 \times VTM - 7.011 \quad (13)$$

Dynamic Modulus of ATPB

The dynamic modulus test, with modifications as previously discussed, was used to determine the stiffness of the ATPB specimens at varying air void contents. During the test, three replicate specimens having an air void content within 1% of the average were considered as a group for each air void content. The average modulus value from each temperature and frequency combination for the replicates was used to construct master curves. The average dynamic modulus values at the 10 Hz test frequency are shown in Appendix B.

As a viscoelastic material, the stiffness of the asphalt mixture is not only related with the temperature but also the rate of loading. By shifting the dynamic moduli under different temperatures into one smooth curve at a reference temperature (usually 21.1°C), the relationship between the dynamic modulus, temperature and time of loading can be expressed by one single master curve using time-temperature superposition principles. The master curve of dynamic modulus describes the time dependency of the material while the shifting factors at each temperature describe the temperature dependency. The dynamic moduli obtained from tests at various temperatures are shifted with respect to time until the curves merge into a smooth sigmoidal function.[40, 41] There are four parameters in the sigmoidal function that are given as Equation 14 as follows:

$$log|E^*| = \delta + \frac{\alpha}{1+e^{\beta+\gamma(\log t_r)}} \quad (14)$$

Where, t_r is reduced time of loading at reference temperature, α, β, γ, δ are all fitting parameters determined by minimizing errors during curve fitting. The reduced time of loading at a reference temperature is also related to the shift factor as follows:

$$a(T) = \frac{t}{t_r} \quad (15)$$

where $a(T)$ is the shift factor as a function of temperature.

The method which has been adopted to construct the master curve is shown as follows. Firstly, the relationship between the logarithm of the shift factor and the temperature is expressed as a second order polynomial shown as follows:

$$\log a(T_i) = aT_i^2 + bT_i + c \quad (16)$$

Then, by simultaneously solving for the four coefficients of the sigmoidal function (α, β, γ and δ) from Equation 14 and the three coefficients of the second order polynomial (a, b, and c) from Equation 16, the master curve can be constructed. A Microsoft Excel worksheet is often used to conduct the nonlinear optimization for simultaneously solving these seven parameters.

To investigate the influence of the air void content on the dynamic modulus results, all ATPB mixtures were tested using specimens fabricated with different air void contents; the results for the Idaho, Oklahoma, and Virginia mixtures are shown in Figures 20-22, respectively. Generally the dynamic modulus decreased with an increase in air void content. As the stiffness increased (at larger reduced frequencies), the effect of air void content was found to increase. However, it was noticed that this effect was reduced for the Oklahoma mixtures. When compared to traditional asphalt mixtures that might have a dynamic modulus of approximately 7000 MPa at a reduced frequency of 1.0 Hz, the dynamic modulus of the drainage layer materials was much lower.[42] The laboratory-determined dynamic modulus of ATPB specimens suggests that the ATPB drainage layer is possibly a weak load bearing layer within pavement structure.

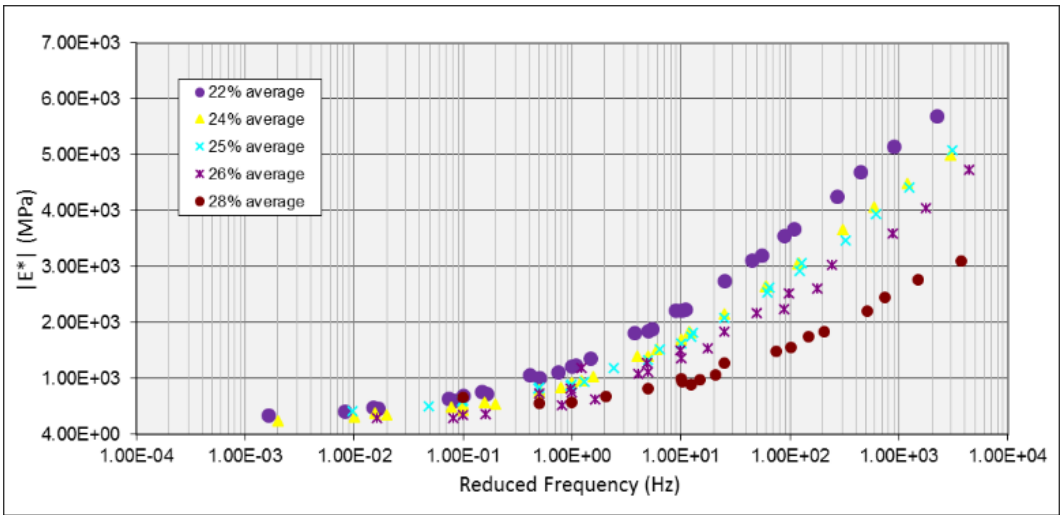

Figure 20. Dynamic Modulus Master Curves for Idaho ATPB Mixtures Having Different Air Void Contents.

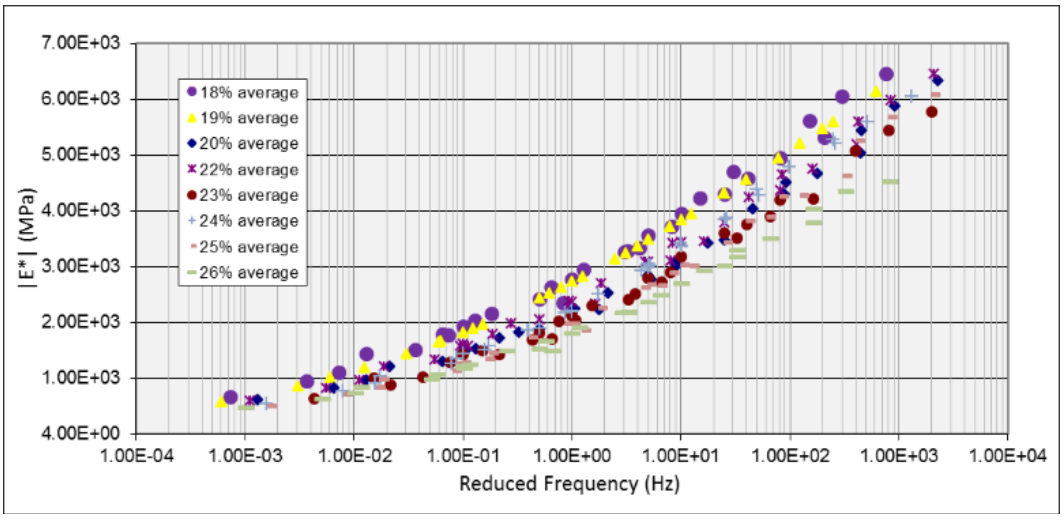

Figure 21. Dynamic Modulus Master Curves for Oklahoma ATPB Mixtures Having Different Air Void Contents.

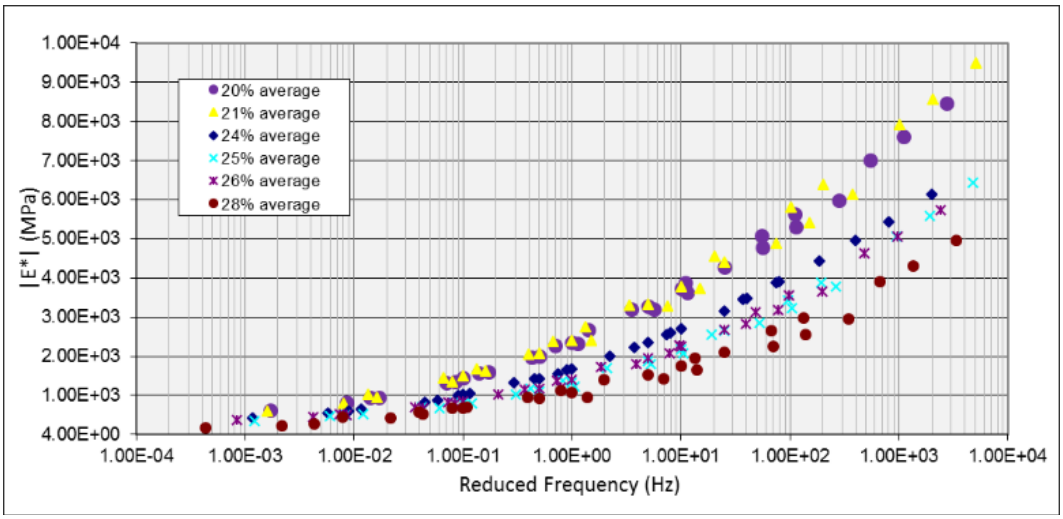

Figure 22. Dynamic Modulus Master Curve of Virginia ATPB Specimens Having Different Air Void Contents.

Calibrated NCHRP 1-37A Model to Predict Dynamic Modulus of ATPB

Another method to determine the dynamic modulus of ATPB materials is by use of prediction equations included in the AASHTO Pavement-ME software. The prediction model, developed under NCHRP project 1-37A, uses a regression model to predict the dynamic modulus from more commonly available mixture parameters, such as the aggregate gradations, asphalt binder properties and volumetric properties of the mixture and is shown as follows[43]:

$$\log E^* = -1.249937 + 0.029232\rho_{200} - 0.001761(\rho_{200})^2 - 0.002841\rho_4 - \\ -0.058097V_a - 0.082208\frac{V_{beff}}{V_{beff}+V_a} \\ + \frac{3.871977 - 0.0021\rho_4 + 0.003958\rho_{3/8} - 0.000017\left(\rho_{3/8}\right)^2 + 0.005470\rho_{3/4}}{1+e^{(-0.603313-0.313351\log(f)-0.393532\log(\eta))}} \quad (17)$$

Where

E^* = dynamic modulus of mix, 10^5 psi;
η = binder viscosity, 10^6 poise;
f = loading frequency, Hz;
ρ_{200} = % passing #200 sieve;
ρ_4 = cumulative % retained on #4 sieve;
$\rho_{3/8}$ = cumulative % retained on 3/8 in. sieve;
$\rho_{3/4}$ = cumulative % retained on 3/4 in. sieve;
V_a = % air voids, by volume; and
V_{beff} = % effective binder content, by volume.

The effective binder content V_{beff} is calculated as follows:[44]

$$V_{beff} = G_{mb}\left[\frac{P_b}{G_b} - (100 - P_b)\frac{G_{se} - G_{sb}}{G_{se} \times G_{sb}}\right] \quad (18)$$

Where

G_{mb} = bulk specific gravity of the mix;
Pb = binder content by weight;
Gb = specific gravity of the binder at 60°F;
G_{se} = effective specific gravity of the aggregate;
$G_{se} = \frac{100 - Pb}{\frac{100}{G_{mm}} - \frac{Pb}{Gb}}$; and
G_{sb} = bulk specific gravity of the aggregate.

The effective binder content V_{beff} was calculated for ATPB mixtures from Idaho, Oklahoma, and Virginia as is shown in Table 10. The binder viscosity, η, is determined within the AASHTO Pavement-ME software by selecting the appropriate binder performance grade.

Table 10a. Effective Binder Contents for Virginia ATPB Specimens

ATPB-VA 20%										
P_b	G_b	G_{mm}	G_{se}	G_{sb}	G_{mb}			V_{beff}		
					A1*	A2	A3	A1	A2	A3
4.3	1.011	2.474	2.646	2.578	1.975	1.970	1.970	6.515	6.497	6.498
ATPB-VA 21%										
P_b	G_b	G_{mm}	G_{se}	G_{sb}	G_{mb}			V_{beff}		
					A5	A6	A1-1	A5	A6	A1-1
4.3	1.011	2.474	2.646	2.578	1.954	1.951	1.957	6.447	6.437	6.455
ATPB-VA 24%										
P_b	G_b	G_{mm}	G_{se}	G_{sb}	G_{mb}			V_{beff}		
					B2	B3	B2-2	B2	B3	B2-2
4.3	1.011	2.474	2.646	2.578	1.889	1.876	1.869	6.232	6.187	6.164
ATPB-VA 25%										
P_b	G_b	G_{mm}	G_{se}	G_{sb}	G_{mb}			V_{beff}		
					B4	B1-1	B1-2	B4	B1-1	B1-2
4.3	1.011	2.474	2.646	2.578	1.851	1.857	1.850	6.107	6.127	6.101
ATPB-VA 26%										
P_b	G_b	G_{mm}	G_{se}	G_{sb}	G_{mb}			V_{beff}		
					B1	B5	B6	B1	B5	B6
4.3	1.011	2.474	2.646	2.578	1.837	1.821	1.839	6.060	6.008	6.065
ATPB-VA 28%										
P_b	G_b	G_{mm}	G_{se}	G_{sb}	G_{mb}			V_{beff}		
					C3	C4	C1-1	C3	C4	C1-1
4.3	1.011	2.474	2.646	2.578	1.773	1.792	1.788	5.849	5.910	5.899

*Note: A1, A2, A3, etc. are specimen numbers.

Table 10b. Effective Binder Contents for Oklahoma ATPB Specimens

ATPB-OK 18%										
P_b	G_b	G_{mm}	G_{se}	G_{sb}	G_{mb}			V_{beff}		
					E1*	E3	E6	E1	E3	E6
2.5	1.030	2.524	2.621	2.680	2.055	2.072	2.071	6.663	6.719	6.718
ATPB -OK 19%										
P_b	G_b	G_{mm}	G_{se}	G_{sb}	G_{mb}			V_{beff}		
					E2	E4	E5	E2	E4	E5
2.5	1.030	2.524	2.621	2.680	2.050	2.051	2.053	6.649	6.652	6.658
ATPB -OK 20%										
P_b	G_b	G_{mm}	G_{se}	G_{sb}	G_{mb}			V_{beff}		
					E7	E8	F3	E7	E8	F3
2.5	1.030	2.524	2.621	2.680	2.013	2.011	2.027	6.528	6.523	6.573
ATPB -OK 22%										
P_b	G_b	G_{mm}	G_{se}	G_{sb}	G_{mb}			V_{beff}		
					F1	F7	G3	F1	F7	G3
2.5	1.030	2.524	2.621	2.680	1.970	1.969	1.964	6.389	6.387	6.369
ATPB -OK 23%										
P_b	G_b	G_{mm}	G_{se}	G_{sb}	G_{mb}			V_{beff}		
					G1	G2	G7	G1	G2	G7
2.5	1.030	2.524	2.621	2.680	1.955	1.946	1.936	6.342	6.312	6.280
ATPB -OK 24%										
P_b	G_b	G_{mm}	G_{se}	G_{sb}	G_{mb}			V_{beff}		
					H1	H3	H5	H1	H3	H5
2.5	1.030	2.524	2.621	2.680	1.908	1.917	1.912	6.187	6.217	6.200
ATPB -OK 25%										
P_b	G_b	G_{mm}	G_{se}	G_{sb}	G_{mb}			V_{beff}		
					H4	H7	I3	H4	H7	I3
2.5	1.030	2.524	2.621	2.680	1.885	1.899	1.894	6.113	6.158	6.143
ATPB -OK 26%										
P_b	G_b	G_{mm}	G_{se}	G_{sb}	G_{mb}			V_{beff}		
					I2	I4	I5	I2	I4	I5
2.5	1.030	2.524	2.621	2.680	1.880	1.869	1.872	6.097	6.061	6.071

Table 10c. Effective Binder Contents for Idaho ATPB Specimens

ATPB-ID 22%										
P_b	G_b	G_{mm}	G_{se}	G_{sb}	G_{mb}			V_{beff}		
					Q1*	Q2	Q3	Q1	Q2	Q3
3.0	1.030	2.525	2.644	2.569	1.959903	1.949	1.915	3.624	3.604	3.541
ATPB-ID 24%										
P_b	G_b	G_{mm}	G_{se}	G_{sb}	G_{mb}			V_{beff}		
					R1	R4	R5	R1	R4	R5
3.0	1.030	2.525	2.644	2.569	1.914	1.917	1.926	3.540	3.545	3.561
ATPB-ID 25%										
P_b	G_b	G_{mm}	G_{se}	G_{sb}	G_{mb}			V_{beff}		
					S1	S2	S3	S1	S2	S3
3.0	1.030	2.525	2.644	2.569	1.896	1.896	1.894	3.506	3.507	3.502
ATPB-ID 26%										
P_b	G_b	G_{mm}	G_{se}	G_{sb}	G_{mb}			V_{beff}		
					T1	T2	T3	T1	T2	T3
3.0	1.030	2.525	2.644	2.569	1.876	1.851	1.839	3.469	3.423	3.401
ATPB-ID 28%										
P_b	G_b	G_{mm}	G_{se}	G_{sb}	G_{mb}			V_{beff}		
					U2	U4	U5	U2	U4	U5
3.0	1.030	2.525	2.644	2.569	1.827	1.827	1.812	3.377	3.378	3.350

Once all the inputs for the NCHRP 1-37A model have been determined, the dynamic modulus of the ATPB mixtures can be predicted using Equation 17. The predicted E* was compared with the laboratory determined dynamic modulus to see whether this model can be directly applied on the ATPB mixtures. It is found that the predicted dynamic modulus of these mixtures is much lower than the measured values if no modifications were applied to the NCHRP 1-37A model. This is not surprising since the 1-37A model was developed using dense-graded asphalt mixtures.

For each ATPB mixture, a modified dynamic modulus prediction model was developed based on the NCHRP 1-37A model and then calibrated for the ATPB mixture local to each agency. These models can be used to predict the dynamic modulus of ATPB materials from Idaho, Oklahoma, and Virginia at different air void contents in the AASHTO Pavement-ME software.

Since different gradations and control sieves were used by each state to produce the ATPB mixtures, different regional dynamic modulus prediction models were developed for varying air void contents. For example, the gradations of the aggregates used by Idaho's ATPB are controlled using the #8, #4, 3/8 inch, and ½ inch sieves rather than the sieves incorporated in the NCHRP 1-37A model. Three modified dynamic modulus prediction models, including regional sieve sizes as the parameters to predict dynamic modulus, were developed as shown in the following equations.

Idaho ATPB:

$$\log E^* = -1.249885 + 0.029636\rho_8 - 0.000716(\rho_8)^2 + 0.05747\rho_4 - 0.080316V_a - 0.080973\frac{V_{beff}}{V_{beff}+V_a} + \frac{3.857444 - 1.202505\rho_4 - 1.00955\rho_{\frac{3}{8}} + 0.05103\left(\rho_{\frac{3}{8}}\right)^2 - 0.65937\rho_{1/2}}{1+e^{(-0.625196-0.197549\log(f)-0.220528\log(\eta))}} \quad (19)$$

Where, ρ_8 = cumulative percent retained on #8 sieve;

Oklahoma ATPB:

$$\log E^* = -2.93516 + 0.026203\rho_{200} - 0.000663(\rho_{200})^2 - 2.58\times10^{-6}\rho_4 - 0.018256V_a - 0.108905\frac{V_{beff}}{V_{beff}+V_a} + \frac{5.990667 - 0.00535\rho_4 + 0.084364\rho_{\frac{1}{2}} - 1.76\times10^{-5}\left(\rho_{1/2}\right)^2 + 0.043989\rho_1}{1+e^{(-2.15219-0.202076\log(f)-0.202993\log(\eta))}} \quad (20)$$

Where, ρ_1 = cumulative percent retained on 1 inch sieve;

Virginia ATPB:

$$\log E^* = -1.248027 + 0.029956\rho_{200} - 0.000697(\rho_{200})^2 + 0.05277\rho_8 - 0.051533V_a - 0.083203\frac{V_{beff}}{V_{beff}+V_a} + \frac{3.810034 - 1.934289\rho_8 - 3.14479\rho_{\frac{1}{2}} + 0.3782\left(\rho_{\frac{1}{2}}\right)^2 - 0.48496\rho_{3/4}}{1+e^{(-0.64184-0.197242\log(f)-0.225136\log(\eta))}} \quad (21)$$

The laboratory measured versus predicted E* data using Equations 19-21 are shown in Figures 23-25, respectively.

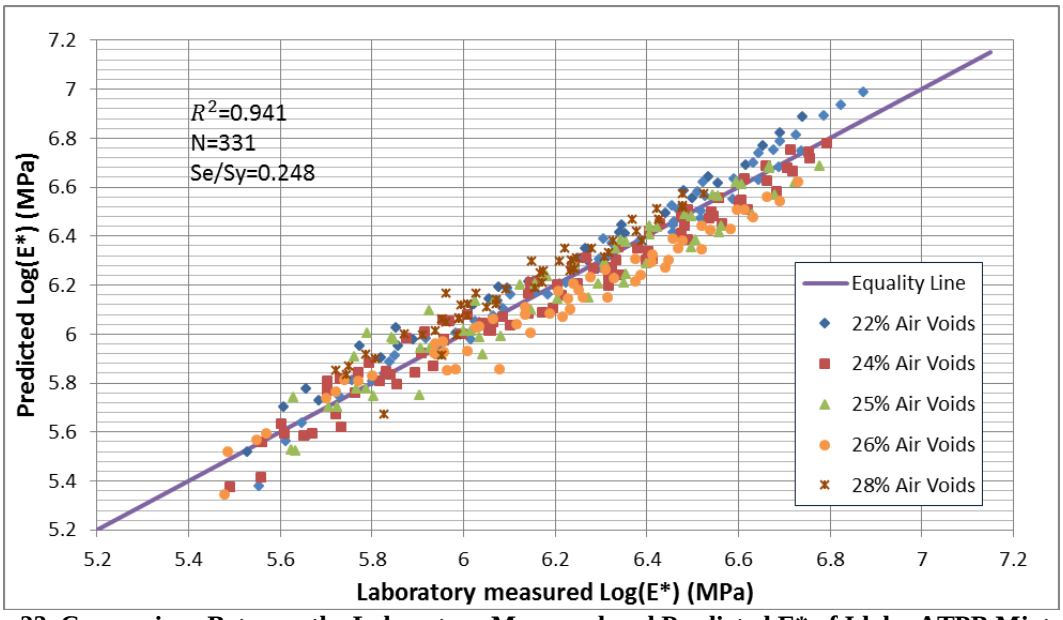

Figure 23. Comparison Between the Laboratory Measured and Predicted E* of Idaho ATPB Mixture by Modified Regional NCHRP 1-37A Model at Different Air Void Contents.

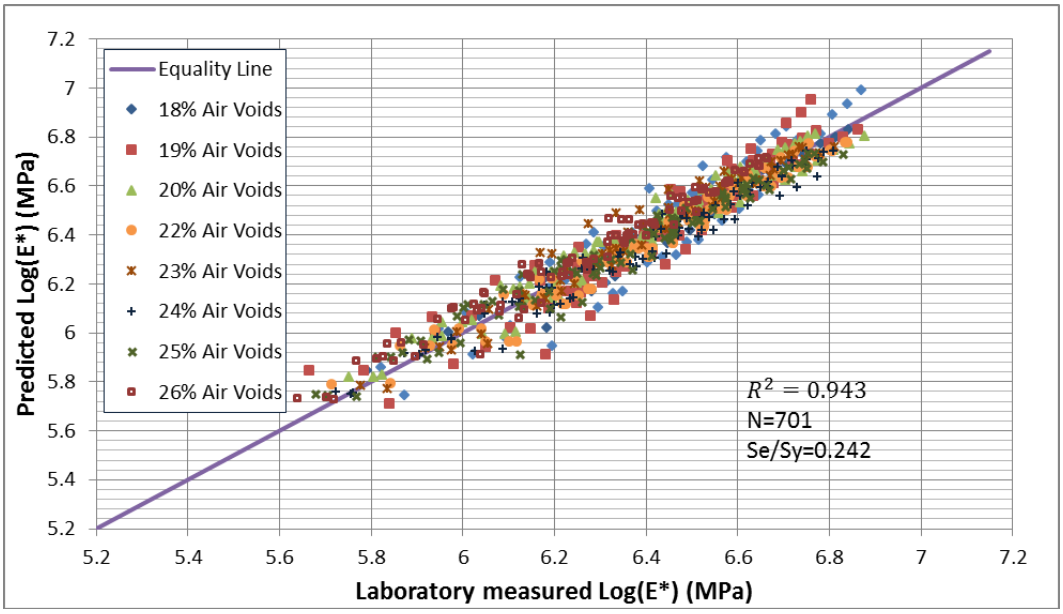

Figure24. Comparison Between the Laboratory Measured and Predicted E* of Oklahoma ATPB Mixture by Modified Regional NCHRP 1-37A Model at Different Air Void Contents.

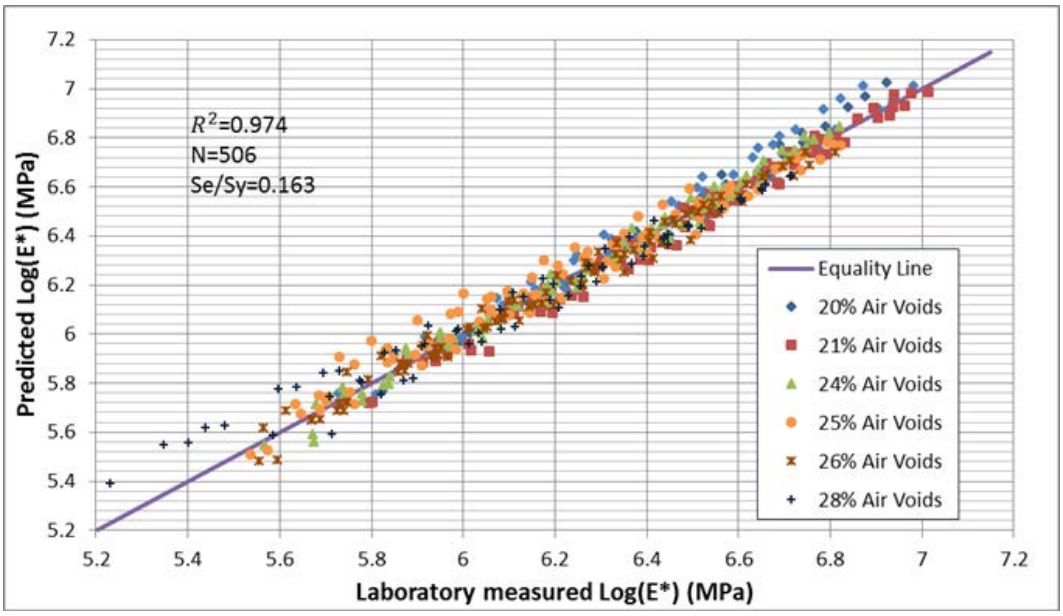

Figure 25. Comparison Between the Laboratory Measured and Predicted E* of Virginia ATPB Mixture by Modified Regional NCHRP 1-37A Model at Different Air Void Contents.

By visual observation of Figures 23-25, the modified regional NCHRP 1-37A models predict the laboratory measured dynamic modulus very well. Table 11 includes details on additional goodness-of-fit statistics.

Table 11. Goodness-of-Fit Statistics for Modified Regional NCHRP 1-37A Models

	Standard Error, S_e	**Sum of Squared Error, SSe**	**Standard Deviation, S_y**	**S_e/S_y**	**Correlation Coefficient, R^2**	**Number of data points, N**
Idaho	0.082	2.134	0.331	0.248	0.941	331
Oklahoma	0.064	2.794	0.266	0.241	0.943	701
Virginia	0.057	1.165	0.350	0.163	0.974	506

The ratio of S_e/S_y is an indicator of how the modified regional model improves the accuracy of the prediction; the smaller the ratio of S_e/S_y is, the better the prediction is. The correlation coefficient (R^2) also measures accuracy of the calibrated model with a better prediction shown the closer R^2 is to one. It has been found that R^2 is a better indicator for linear models with a large sample size while the ratio of S_e/S_y is more suitable for non-linear models, such as those shown above, to evaluate the predictive ability of the model.[45] As shown in Table 12, all of the three modified regional models exhibit a high predictive ability.

In addition to the modified regional models, a more general modified NCHRP 1-37A model was developed to predict the dynamic modulus of ATPB specimens that is independent of location. Based on the test results shown above, an overall model that can be used for different ATPB mixtures with different aggregate gradations, asphalt binder types and air void contents was developed. To develop such a model, the laboratory-determined dynamic modulus from the three mixtures with different air void contents was used; the dataset included approximately 1,538 data points from 57 specimens tested at five temperatures and six frequencies. The general modified NCHRP 1-37A model is shown as follows:

$$\log E^* = -5.363 \times 10^{-4} - 0.505\rho_{200} + 1.709(\rho_{200})^2 + 3.978 \times 10^{-4}\rho_4 - 0.132V_a$$
$$-10.382\frac{V_{beff}}{V_{beff}+V_a} + \frac{-50.640+3.506\times10^{-5}\rho_4+2.275\rho_{3/8}+0.013(\rho_{3/8})^2-6.989\rho_{3/4}}{1+e^{(-1.664-0.141\,log(f)-0.0152\,log(\eta))}} \quad (22)$$

The laboratory measured versus predicted E* data using Equation 22 are shown in Figure 26. By visual observation of Figure 26, the general modified NCHRP 1-37A model predicts the laboratory measured dynamic modulus very well. Table 12 includes details on additional goodness-of-fit statistics.

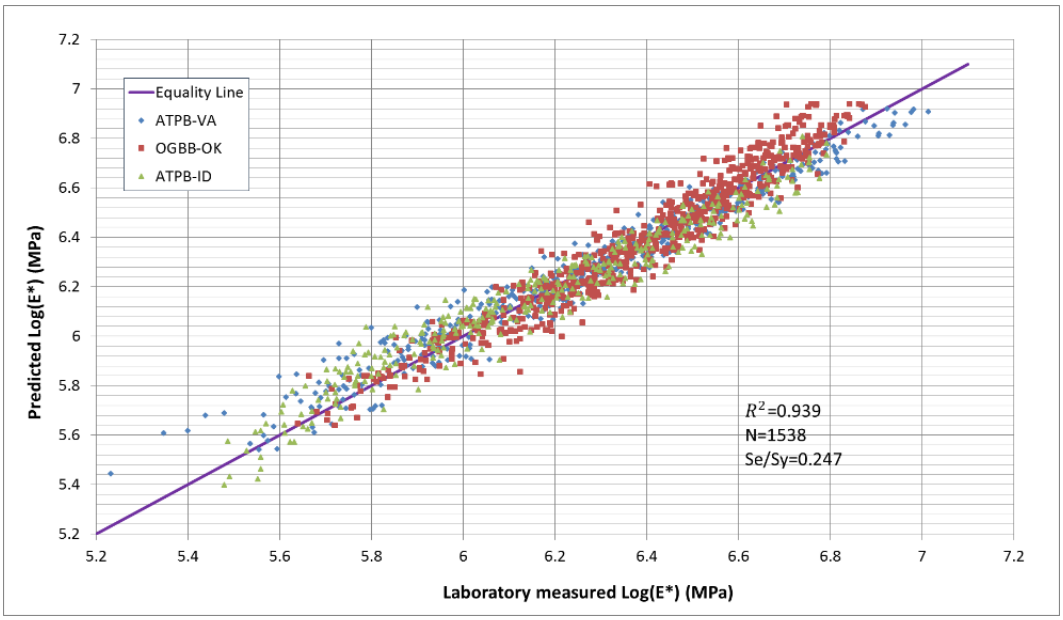

Figure 26. Comparison between the Laboratory Measured and Predicted E* of All ATPB Mixtures by General Modified NCHRP 1-37A Model.

Table 12. Goodness-of-Fit Statistics for General Modified NCHRP 1-37A Model

	S_e/S_y	SS_e	S_e	R^2	N
Equation 28	0.247	8.921	0.076	0.939	1538

Compressive Strength of Oklahoma CTPB Mixtures

Twenty-four CTPB specimens from Oklahoma were fabricated having an air void content range of 26% to 34%. Since the specimens were compacted in their molds by hand-rodding, the least air void content achieved was 26%. After fabrication, the specimens were cured and stored until compressive strength testing at 7, 14, 21, and 28 days. The compressive strength of the CTPB specimens is shown in Figure 27. Each data point below represented one CTPB specimen.

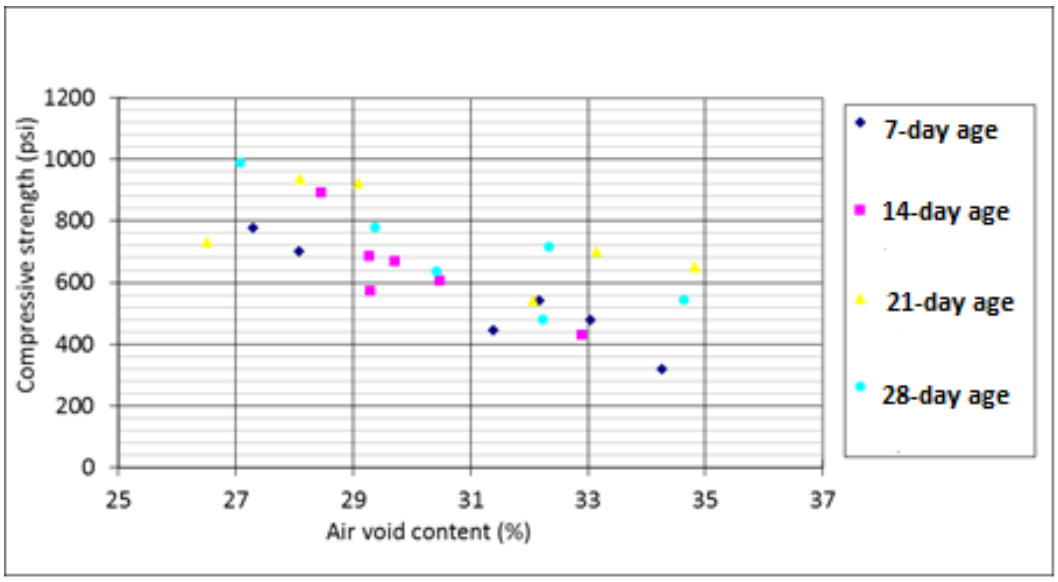

Figure 27. Compressive Strength Versus Air Void Content for CTPB Specimens at 7, 14, 21, and 28 Days.

From Figure 27, it can be seen that the compressive strength decreases as the air void content increases, with each data point showing one specimen at different ages and air void contents. Generally, the compressive strength of the CTPB specimens increases with age. When compared with the default hydraulic cement concrete strength values in the AASHTO Pavement-ME software, the compressive strengths of the CTPB specimens are much lower as expected. Therefore, if the drainage layer will be considered as a structural layer and included in the structural design in the AASHTO Pavement-ME process, proper compressive strengths of the CTPB mixtures should be used. Based on these results, the recommended default compressive strength of the CTPB mixtures range from 400 psi to 1000 psi.

Resilient Modulus of Wisconsin UPB

The resilient modulus of granular materials is typically influenced by material type, physical properties of the sample including density and moisture content, and the stress state. Since the influence of moisture content on the coarse-grained material is not as significant as fine-grained material due to less suction effects, the influence of moisture content on the resilient modulus is not discussed here in this study. All the UPB samples are at 10% volumetric moisture content. Figure 28 and Figure 29 illustrate the resilient modulus of sample No.1 with 15% air void content and sample No.2 with 20% air void content versus cyclic stress, respectively. Appendix C presents results from Discrete Element Method (DEM) simulation to investigate the performance of UPB at higher air void contents.

As can be seen from Figure 28 and Figure 29, a linear relationship between resilient modulus and cyclic stress is observed on a logarithmic plot. Secondly, with increasing confining pressure and cyclic stress as adopted by successive load sequences during the test, the samples are condensed gradually and have shown increasing resilient modulus values. In addition, the effects of confinement are greater than that of the cyclic stress regarding resilient modulus for the UPB material. Therefore, it is more important to ensure accurate confining pressures during the laboratory resilient modulus test to achieve reasonable results in this case.

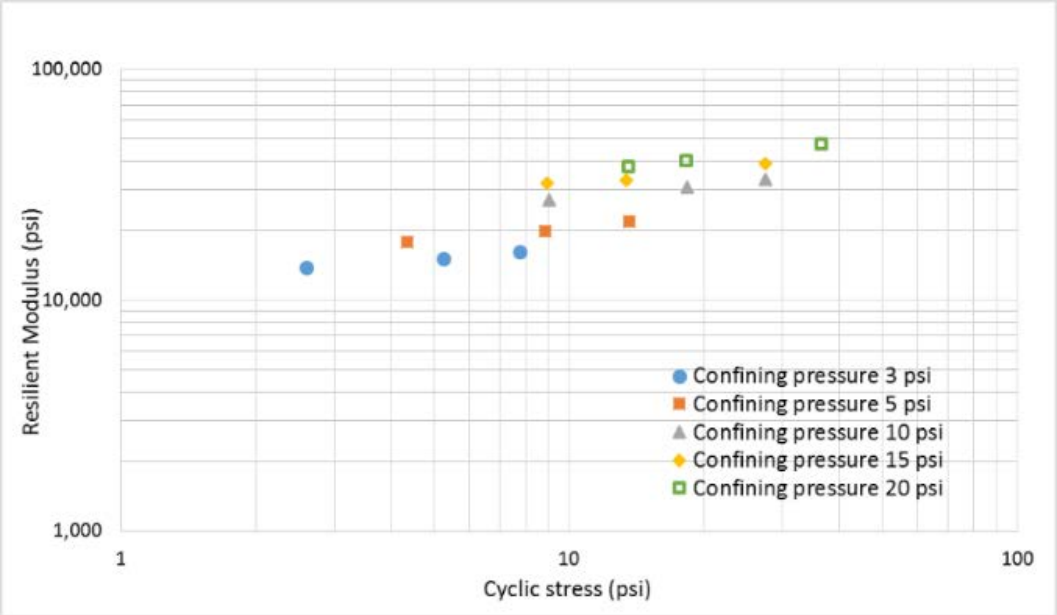

Figure 28. Logarithmic Plot of Resilient Modulus Versus Cyclic Stress of Specimens with 15% Air Void Content.

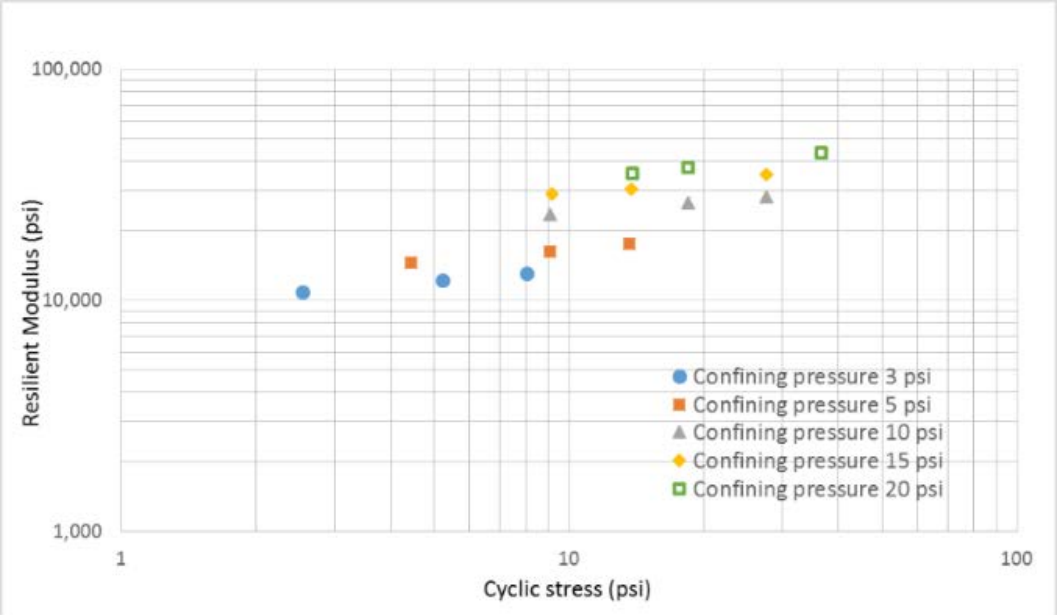

Figure 29. Logarithmic Plot of Resilient Modulus Versus Cyclic Stress of Specimens with 20% Air Void Content.

There are several resilient modulus prediction models available for both fine and coarse granular materials, taking into consideration factors such as cyclic stress, confinement, stress state and so forth. Three of the typical prediction models suitable for coarse granular materials, including the modified LTPP model and the MEPDG model are adopted in this study and the regression constants are determined through fitting the laboratory data into the prediction models with the smallest sum of squares for error. Table 13 lists the regression constants of the UPB material in accordance with these models.

Table 13. Regression Constants and Goodness-of-Fit Statistics of Resilient Modulus Prediction Models

Prediction model	$M_R = K_1(S_c)^{K_2} \cdot (S_3)^{K_5}$				
	K1	K2	K5	S_e/S_y	R^2
Specimen# 1	7043.369	0.201	0.388	0.0490	0.998
Specimen# 2	4990.332	0.185	0.495	0.0456	0.998
Prediction model	LTPP: $\text{Log}\left(\frac{M_R}{p_a}\right) = k_1 + k_2 log\left(\frac{\theta}{p_a}\right) + k_3 log\left(\frac{\tau_{oct}}{p_a}\right) + k_4\left[log\left(\frac{\tau_{oct}}{p_a}\right)\right]^2$				
	k1	k2	k3	k4	S_e/S_y	R^2
Specimen# 1	3.017	0.576	0.000	0.000	0.0575	0.997
Specimen# 2	2.916	0.661	0.000	0.000	0.0761	0.994
Prediction model	MEPDG: $M_R = k_1 P_a \left(\frac{\theta}{p_a}\right)^{k_2}\left[\left(\frac{\tau_{oct}}{p_a}\right)+1\right]^{k_3}$				
	k1	k2	k3	S_e/S_y	R^2
Specimen# 1	1022.880	0.591	0.000	0.0681	0.995
Specimen# 2	801.165	0.698	-0.0357	0.0688	0.995

Accompanying quick shear tests were also conducted at end of the resilient modulus test. The samples were left in the same apparatus and an axial load at a strain rate of 1% per minute was applied on the sample until failure occurred or the total axial strain reached 5%. The confining pressure was 5 psi. The test can be seen as under un-drained condition considering the loading was applied at a fast rate. During the entire quick shear test, the axial stress was recorded to investigate the relationship between axial stress and strain. Figure 30 has shown the measured axial stress-strain relationship for the two samples. It can be seen from Figure 30 that the shear strength at failure for the two samples with 15% and 20% air void content is 320 kPa and 230 kPa respectively under 5 psi confinement. With increasing air void content of 5%, the shear strength has dropped by nearly 28%.

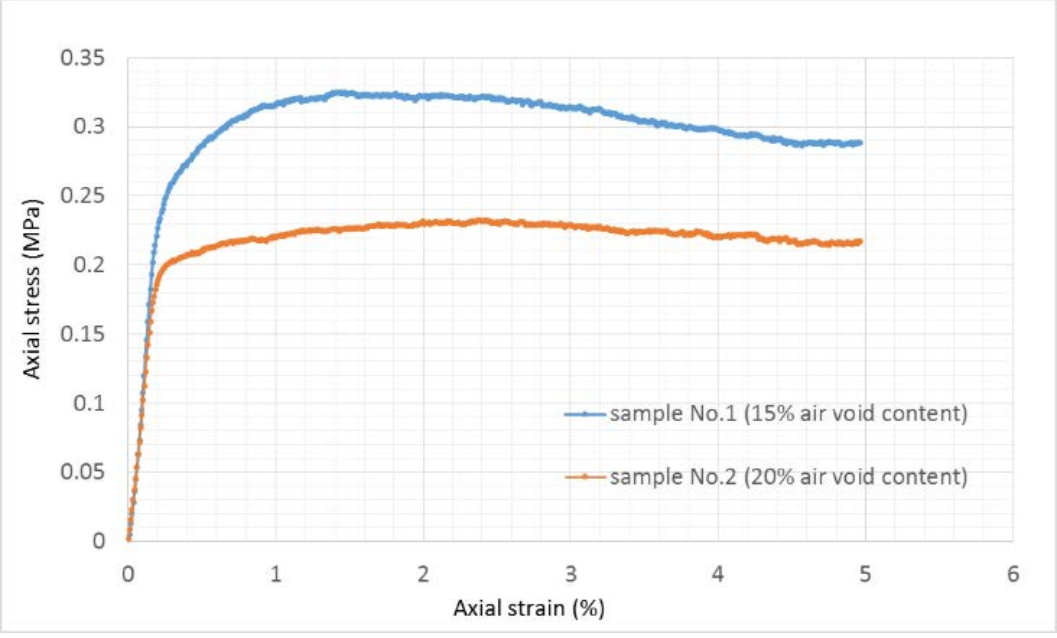

Figure 30. Axial Stress Versus Strain from Quick Shear Test.

Previous studies have already found that there are strong linear correlations between the resilient modulus and the axial stress at 1% strain in quick shear test for fine and coarse soils.[46] However, the correlations are not suitable for the Wisconsin UPB materials based on investigation in this study. The considerable difference between the prediction (from correlation with the axial stress at 1% strain) and measured resilient modulus indicates the need to construct new models between the resilient modulus and the axial stress at 1% strain in a quick shear test for the unbound open graded drainage layer mixes.

Computer Modeling Results

Finite Element Modeling to Evaluate Structural Contribution and Location of Drainage Layer

Generally, the structural performance of the drainage layer is not considered by most pavement analysis and design procedures. Due to its particular material properties, as compared with dense-graded asphalt mixtures, the stress and strain distribution within the pavement structure may change significantly when a drainage layer is used. Finite Element Method (FEM) was used to investigate the structural contribution and the location effect of the drainage layer. The MEPDG is used to determine the upper and lower bounds of the optimal air void content in terms of both sufficient permeability and good structural performance.

Prony Series Parameters

The Prony series are used to mechanically describe the time-temperature dependent properties of asphalt mixtures and to incorporate realistic material properties into FEM simulations. Equation 23 shows the storage modulus (imaginary part) in form of frequency domain Prony series. This mathematical model becomes more accurate in describing the laboratory testing data as more terms are included. According to the investigation in this study, by increasing the terms in Prony series from 5 to 11, the model approaches the original test data as shown in Figure 31.

$$E'(\omega) = G_0\left[1 - \sum_{i=1}^{n} \overline{g_i^P}\right] + G_0 \sum_{i=1}^{n} \frac{\omega^2 \tau_i^2 \overline{g_i^P}}{\omega^2 \tau_i^2 + 1} \quad (23)$$

where
$E'(\omega)$ is the imaginary part of the complex modulus, or storage modulus, and
G_0, $\overline{g_i^P}$, τ_i are all coefficients.

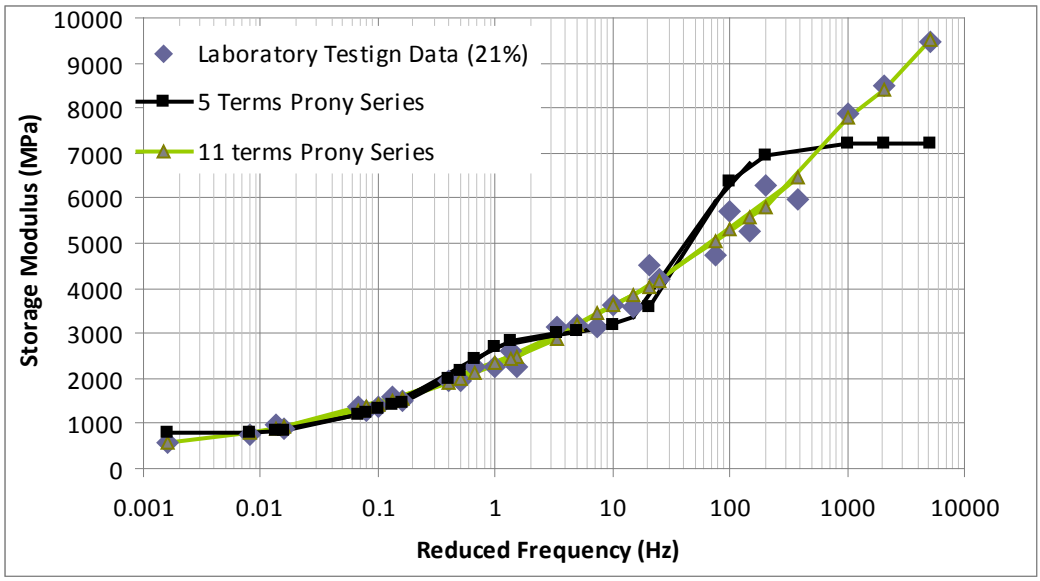

Figure 31. The Prony Series with 5 and 11 Terms (Virginia ATPB with 21% air voids).

Considering the increased accuracy, the fitted parameters of the 11-term Prony series were used in the FEM simulation to describe the time-temperature properties of the ATPB materials.

Simulated Pavement Structure

Compared with static loading and multi-layer elastic theory, FEM simulation considering dynamic loading and realistic material properties are more accurate and can provide the closest pavement responses to field measured results. [47, 48] A flexible pavement model, based on the pavement structure used on the Franklin Turnpike Extension at Lynchburg, Virginia was analyzed. The pavement model measures 5 meters in the direction of traffic. The configuration of the pavement model and the contact area are shown in Figure 32.

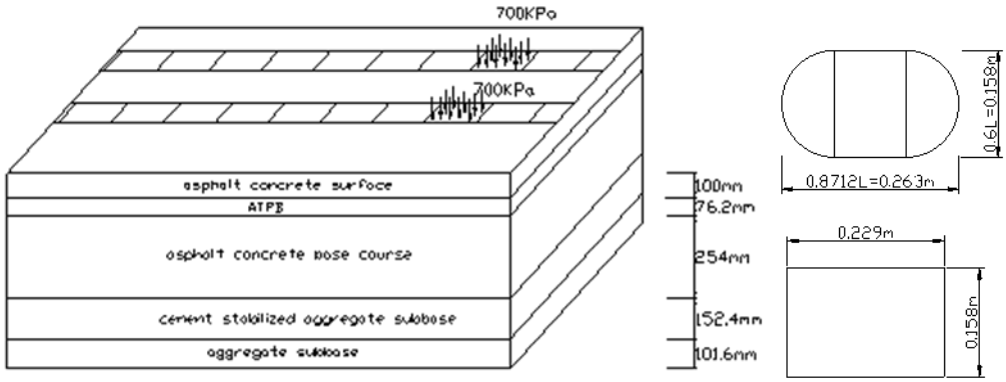

Figure 32. Configuration of the Pavement Model and Contact Area.

The air void content of the ATPB drainage layer was assumed to be 25% in the simulation. The Prony series parameters representing the viscoelastic properties of the ATPB

drainage layer at 25% air void content were used in Dynamic/Implicit analysis. A moving half-sinusoidal traffic loading was applied on the surface of the pavement model at speed of 40 mph. The magnitude of the tire-pavement contact pressure was 700 kPa. Table 14 has listed the material properties used in the simulation.

Table 14. Summary of Material Parameters in FEM simulation

Layer	Thickness (mm)	Elastic modulus (MPa)	Poisson's Ratio
AC surface layer	100	3500	0.30
AC Base	254	3000	0.30
ATPB	76.2	352 (long term)	0.30
Cement treated subbase	152.4	1400	0.30
Aggregate subbase	101.6	200	0.35

Location and Presence of Drainage Layer

The influence of the location and presence of an ATPB layer was studied by comparing the simulated response of three trials. The trials included placing the ATPB above and below the asphalt base layer, and removing the ATPB completely.

The stress and vertical deformation on the surface of pavement versus time showed that the maximum stress and vertical deformation happened at about 0.001 seconds after the wheel loading reached the maximum values. As the wheel load passed, the stress and strain dissipated dramatically. The damping of the stress, however, was much faster than that of the deformation as found in another study.[49] Although no notable differences were observed in stress and deformation on the surface of the pavement in the time domain, large differences were found along the depth right below the wheel at the end of the traffic loading, as shown in Figure 33 to Figure 35. The vertical deformations under wheel loading are comparable when the drainage layer is located above or below the base as shown in Figure 33. The total vertical deformation at surface under wheel loading is slightly larger when the drainage layer is located above the base. The horizontal tensile stress at the top of the drainage layer is always the largest whether the drainage layer is located above or below the base course as illustrated in Figure 34. Figure 35 demonstrates that the vertical stress within the surface and drainage layer is larger in the above base case.

The pavement structure without the ATPB drainage layer was also simulated. The mechanical properties of other pavement materials were kept the same. The no-drainage-layer case had the largest vertical deformation at the moment of applying wheel loads as present in Figure 33, indicating that the ATPB drainage layer does undertake part of the load no matter where it is located, although the structural contribution of the drainage layer is not significant.

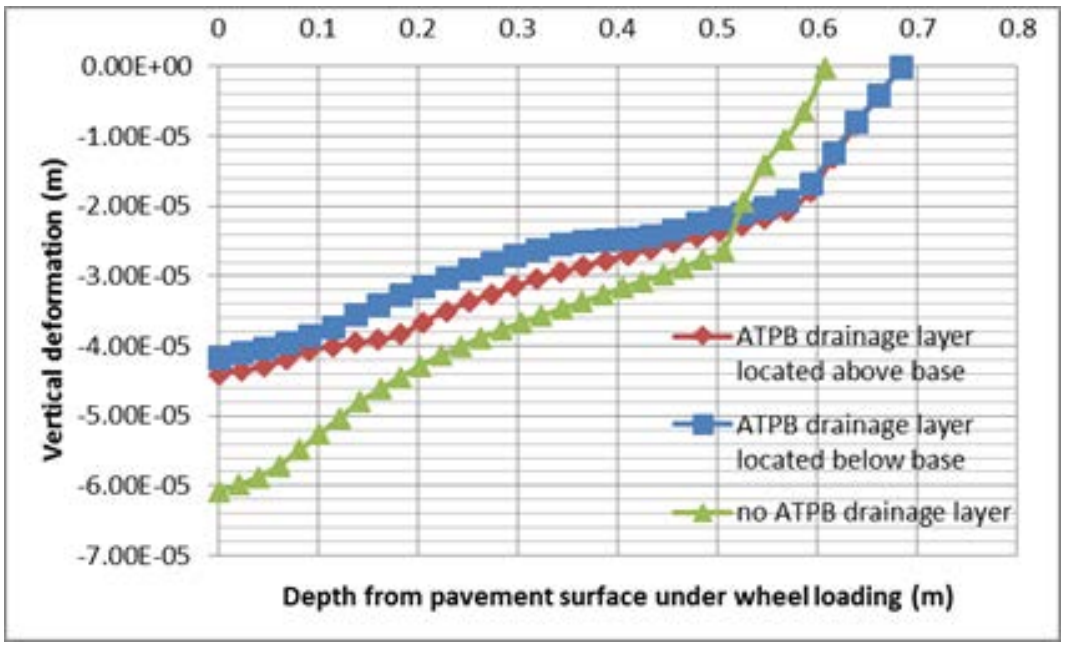

Figure 33. Vertical Deformation Along the Depth Under Traffic Loading.

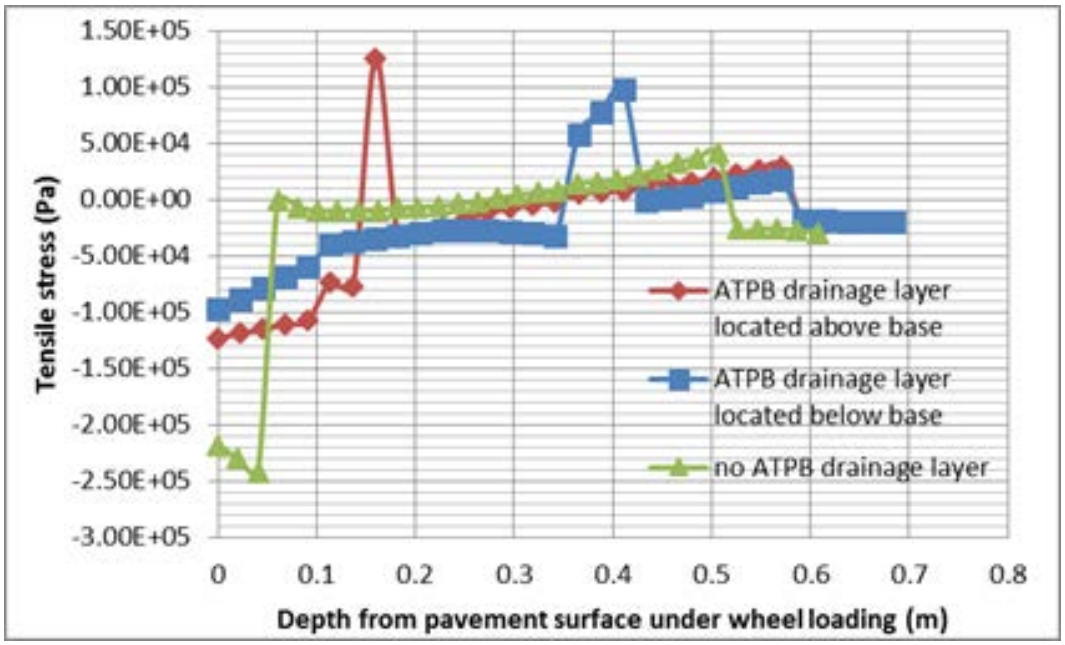

Figure 34. Tensile Stress Along the Depth Under Traffic Loading.

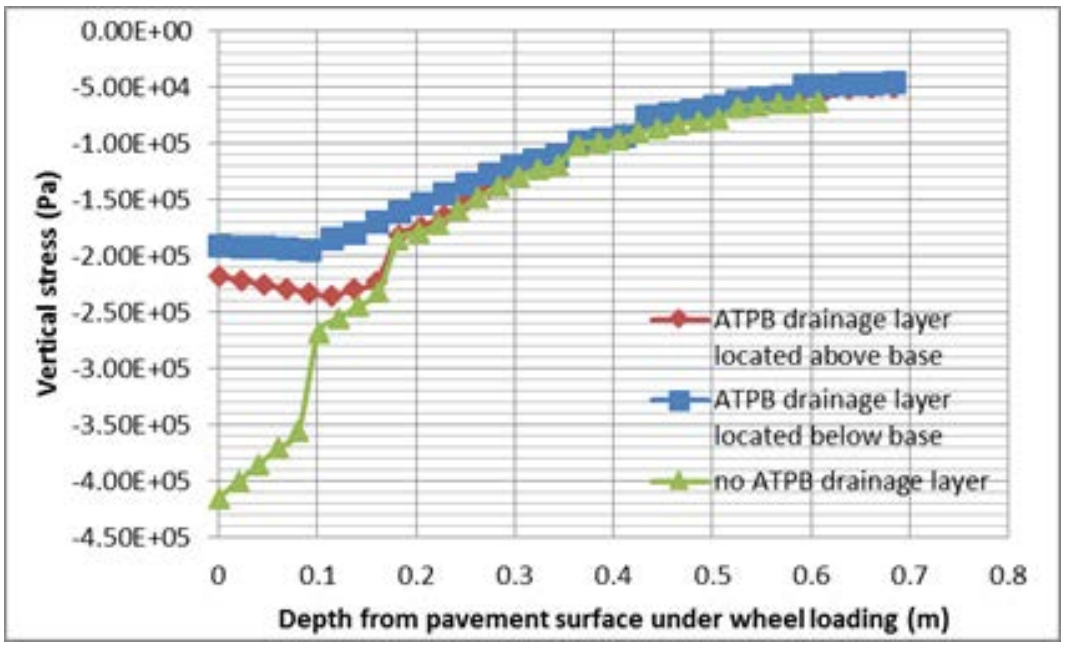

Figure 35. Vertical Stress Along the Depth Under Traffic Loading.

Influence of ATPB Air Void Content

The air void content is an important parameter that influences the mechanical properties of the ATPB layer, given a mixture with the same asphalt binder content and aggregate type. Accordingly, when considering the structural contribution of the ATPB layer, the influence of the air void content should not be neglected. FEM simulations were conducted to investigate the pavement responses with drainage layers having different air void contents under a simulated moving traffic loading.

Based on a comparison between the situations when the drainage layers are of different air void contents, it was found that the stress within the drainage layer is not a monotone-changing function as the air void content changes. This may be attributed to the experimental error of the dynamic modulus or air void content, which are inputs for the simulation. However, generally a pavement with a stiffer ATPB layer, or the ATPB layer with lower air void content, will show a reduced tensile stress from the same loading. Similarly, the vertical stress increases as the air void content of the ATPB layer increases. The distribution of the vertical strain follows the same trend as that of the vertical stress; ATPB layers having a lower air void content will result in lesser deflections at the pavement surface.

Figure 36 to Figure 38 present the influence of the air void content when the ATPB-VA drainage layer is located below the base. The moment when the traffic loading had just passed by was selected as the base for the comparison. Generally the increase in air void content will result in increasing vertical stress, strain and deformation at pavement surface. Similar results have been obtained for the above-base case.

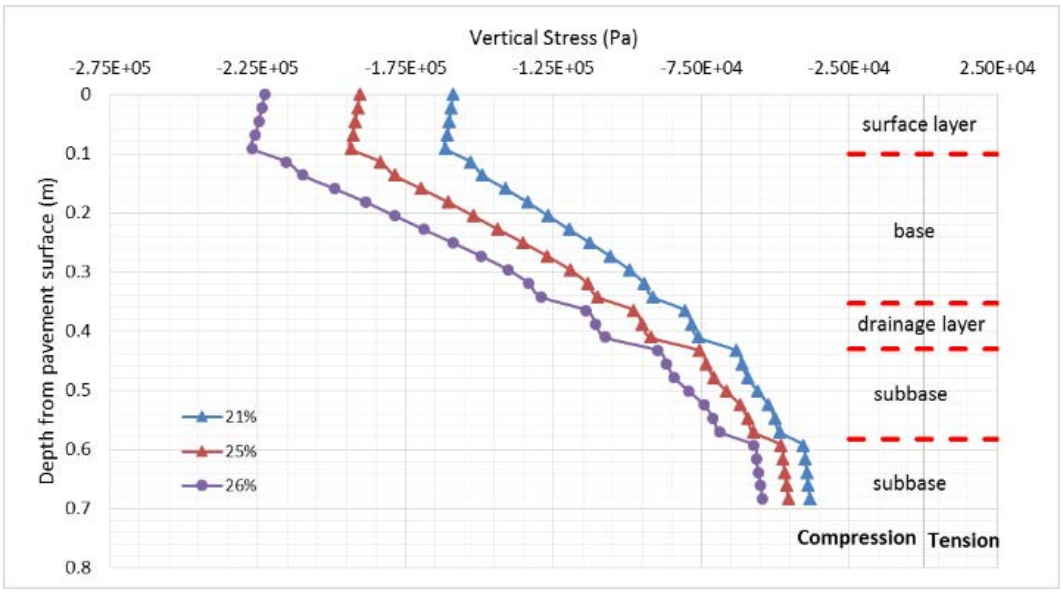

Figure 36. Vertical Stress Distribution Along the Depth Under Traffic Loading with Below-Base Drainage Layer (Virginia ATPB).

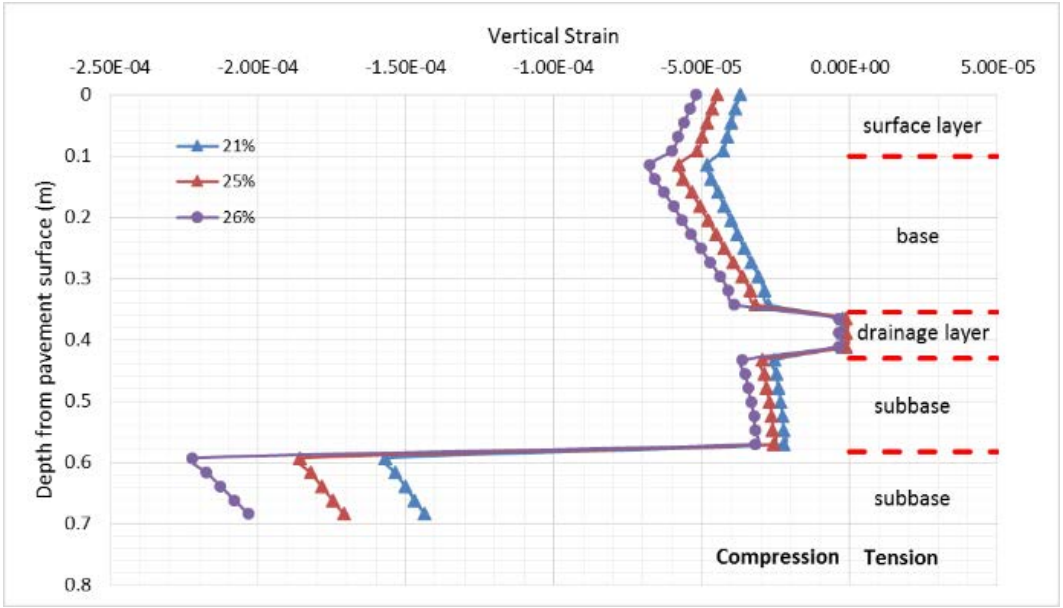

Figure 37. Vertical Strain Distribution Along the Depth Under Traffic Loading with Below-Base Drainage Layer (Virginia ATPB).

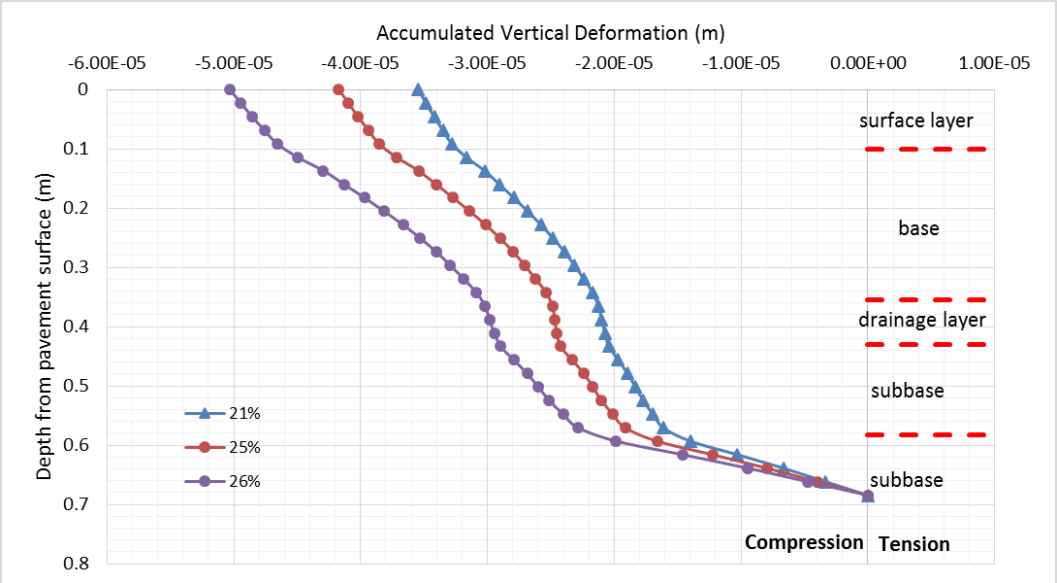

Figure 38. Accumulated Vertical Deformation Distribution Along the Depth Under Traffic Loading with Below-Base Drainage Layer (Virginia ATPB).

Determining an Optimal Air Void Content Range

There are several functions of a drainage layer within a pavement structure. As previously stated, drainage layer systems often contribute both drainage and structural properties, although the structural properties are rarely considered in design. The air void content of the ATPB layer influences not only the permeability, but also the mechanical properties. Increasing in the air void content typically improves the permeability of the drainage layer, but may also reduce the stiffness. Therefore, the selection of an optimal air void content of the ATPB layer is a tradeoff between permeability and stiffness.

According to FHWA, the trend of drainage layers in the 1990s of incorporating a very high permeability of 8,000 to 10,000 ft/day. However, it was found that there is no need to use drainage layers with such high permeability at the price of reducing the stability of the pavement. In addition, the amount of water that can infiltrate into a well-maintained pavement structure does not warrant such a high porosity in the permeable base layer. Per a FHWA document, the current typical permeability of an ATPB drainage layer is from 500 ft/day to 800 ft/day. [50] It should be noted that the current Virginia specification calls for a permeability of 1000 ft/day in permeable drainage layers.[38] The ACPA has also reported the same trend for unstabilized permeable subbases. [51] Taking this into consideration, the criterion of permeability to determine the lower bound of the optimal air void content was selected as 500 ft/day.

Based on laboratory permeability test results, to ensure a permeability of 500 ft/day, the air void content of the ATPB drainage layer materials from Idaho, Oklahoma, and Virginia should be greater than approximately 24%, 21%, and 24.5%, respectively as shown in Figures 20-22. However, it must be determined whether a drainage layer with these air void contents will have adequate strength and stability as part of the pavement structure. As the air void content increases (to achieve good performance in permeability), the stiffness of the drainage layer decreases. To determine the upper bound of the air void content of the drainage layer at which

the stability requirement can be satisfied, a series of simulations were run using the Mechanistic-Empirical Pavement Design Guide (MEPDG) software to predict the potential for rutting at a twenty-year pavement service life. An optimal air void content range can be determined with a lower bound derived from permeability requirement and the upper bound determined from a stability consideration using the MEPDG simulations. One drawback to using the MEPDG software is that the models used to predict distresses from the calculated pavement responses are not locally-calibrated; a change in the calibration factors could change the upper bound of the air void content.

The MEPDG results were analyzed with respect to limiting the total rutting. A threshold value of 0.75 inches was chosen as the limiting distress condition. The pavement structure used in the MEPDG analysis was one used on a recent VDOT project (Franklin Turnpike Extension at Lynchburg, Virginia). Figure 39 presents the pavement structure used in the MEPDG analysis. The ATPB layer was considered as an asphalt concrete layer with the air void content ranging from 20% to 35% in the analysis. The laboratory-determined aggregate gradation and effective binder content of the Virginia ATPB material was used in this analysis. The other inputs for the surface layer, base and subbase follow the typical values for each mixture type. The climate data from Lynchburg, VA was also used.

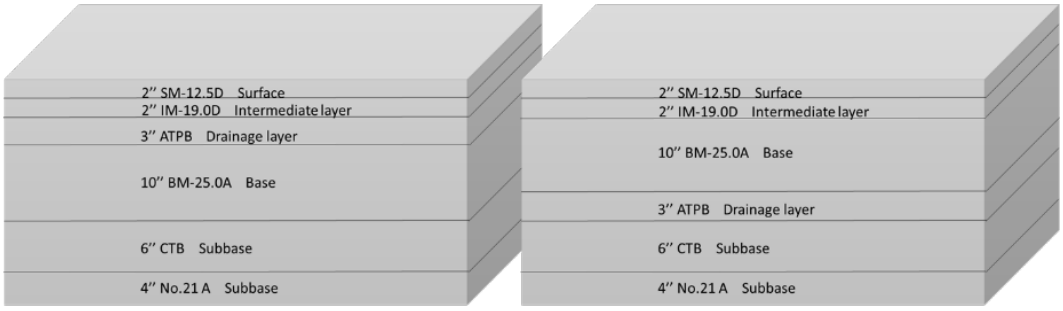

Figure 39. Pavement Structure Used in MEPDG Analysis.

In an MEPDG analysis, the minimum and maximum test temperatures for dynamic modulus testing are recommended in AASHTO standards based on dense-graded asphalt concrete. However, the laboratory-determined dynamic modulus of the Virginia ATPB mixture utilized modified temperatures. As a result, the laboratory-determined dynamic modulus cannot be used as the level 1 inputs in this analysis. On the other hand, because there is no specific prediction model adopted by the MEPDG to consider the mechanical properties of the drainage layer, the calibrated level 2 prediction equations were not used. As a simplified example, the analysis by MEPDG presented here has used the uncalibrated NCHRP 1-37A model to predict the dynamic modulus of the drainage layer. According to the comparison between laboratory-determined and predicted dynamic modulus by NCHRP 1-37A model, the uncalibrated model will underestimate the dynamic modulus of ATPB materials, as previously stated. Therefore the results obtained from this analysis are conservative.

As shown in Figure 40, when the drainage layer is located above the base course, the increase in air void content will increase the permanent deformation during the 20-year service life of the pavement. The pavement incorporated with the Virginia ATPB materials of 25% air void content can survive based on the analysis of 80% reliability. In addition to the criteria of

permanent deformation, surface down cracking is the most susceptible parameter that may exceed the criteria based on the analysis. Figure 41 shows the predicted surface down cracking during the 20-year service life when the drainage layer is located above the base. It is found that the ATPB mixtures with less than 35% air void content all satisfy the surface down cracking requirement with 80% reliability.

Therefore, the lower bound of the optimal air void content of the Virginia ATPB materials has been determined through the laboratory permeability test to be 24.5%, which is the threshold of air void content to reach the 500 ft/day minimum permeability requirement. On the other hand, VDOT specifications require a permeability of 1000 ft/day. Using the equation shown in Figure 16 relating the VTM to the permeability of the ATPB, a VTM of 26.9% would be required.

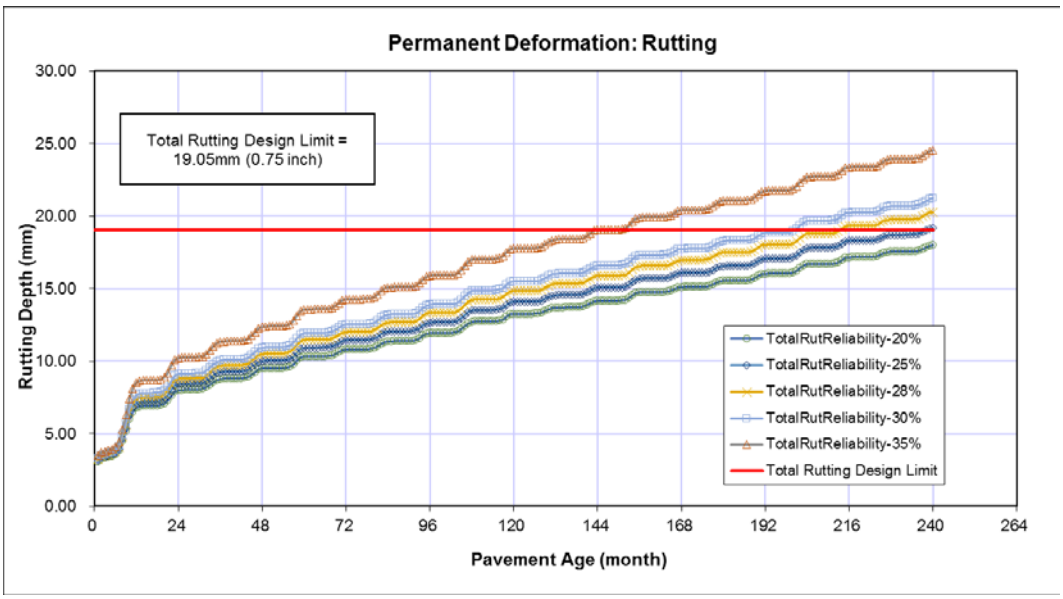

Figure 40. Predicted Rutting During 20-Year Service Life of Pavement with Above-Base ATPB-VA Drainage Layer Having Different Air Void Contents (Virginia ATPB).

The situation when the drainage layer is located below the base layer has also been analyzed using the MEPDG software. Under the 10-inch base layer, the influence of the air void content of ATPB drainage layer on the permanent deformation is not significant. With the air void content of the drainage layer ranging from 20% to 35%, the rutting depth would not exceed 0.75 inch within the given pavement structure during the 20-year service life, according to the 80%-reliability analysis results. The other indicators of pavement performance including surface down cracking, IRI and so forth, all satisfy the requirements when the drainage layer is located below the base. Therefore, it is assumed that as long as the pavement with the ATPB drainage layer located above the base can satisfy all the criteria in M-E design, the pavement with the drainage layer located below the base is also acceptable, given the same material properties.

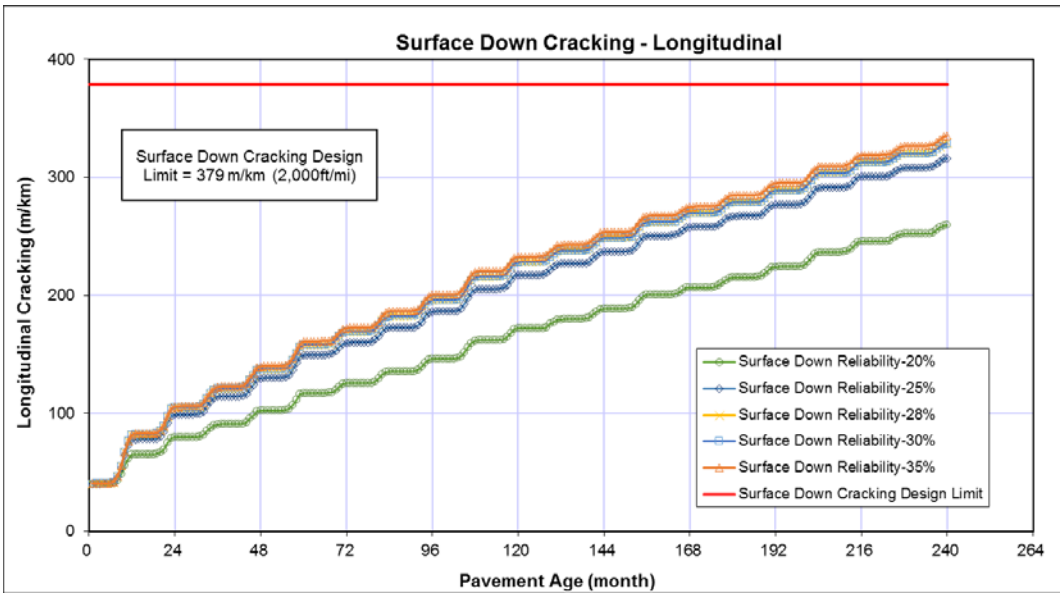

Figure 41. Predicted Surface-Down Cracking During 20-Year Service Life of Pavement with Above-Base ATPB-VA Drainage Layer Having Different Air Void Contents (Virginia ATPB).

Figure 42 to Figure 45 present the MEPDG results from the ATPB from Oklahoma and Idaho for rut depth and surface-down cracking during the pavement service life. The analysis showed a conservative upper bound of the optimal air void content of the Oklahoma ATPB material of 24%, if the same pavement structure is used. For the Idaho ATPB material, the upper bound of the optimal air void content was found to be 28%, with the same pavement structure. Considering the lower bound of the Oklahoma and Idaho materials were 21% and 24%, respectively, as determined from minimum permeability requirement, the optimal air void content ranges were found to be 21% to 24% and 24% to 28% for the Oklahoma and Idaho ATPB materials, respectively. In practice, the pavement structures used may vary with the given pavement structure considered here, which is derived from the Virginia project. Therefore the optimal air void content ranges of the OGBB-OK and ATPB-ID drainage layers provided here may vary with other structures. However, this analysis could be repeated for additional pavement sections. In addition, the distress models used are not locally calibrated. It is possible that using a locally calibrated distress model could change the permeability requirements.

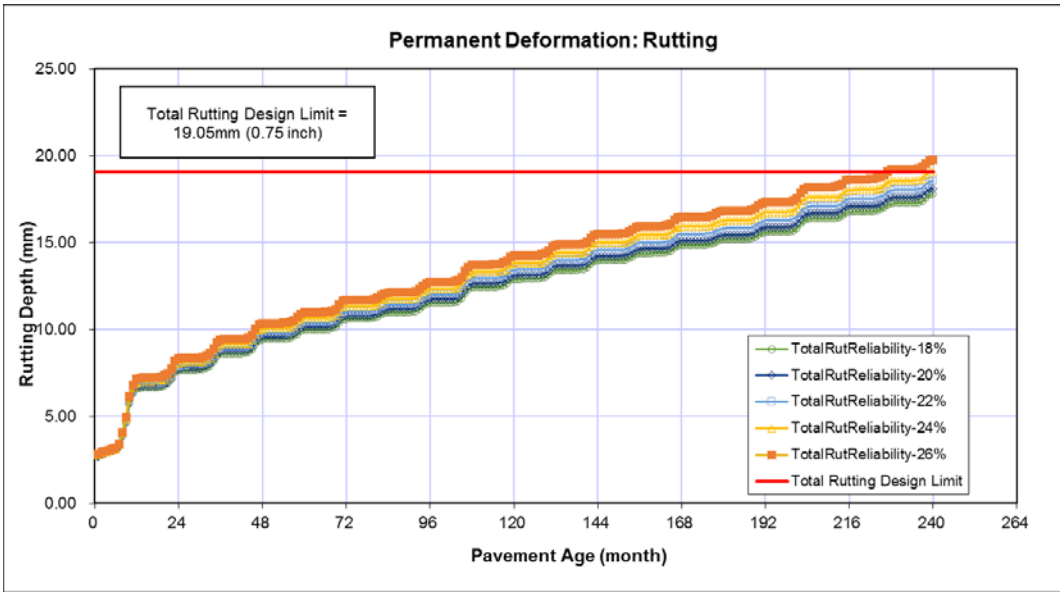

Figure 42.Predicted Rutting During 20-Year Service Life of Pavement with Above-Base Drainage Layer Having Different Air Void Contents (Oklahoma ATPB).

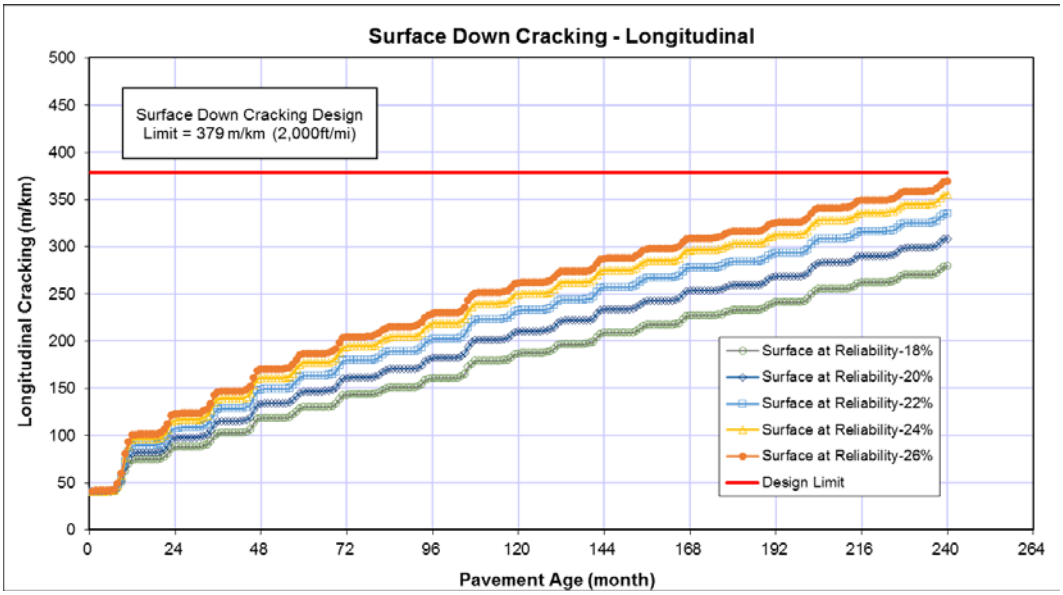

Figure 43. Predicted Surface-Down Cracking During 20-Year Service Life of Pavement with Above-Base Drainage Layer Having Different Air Void Contents (Oklahoma ATPB).

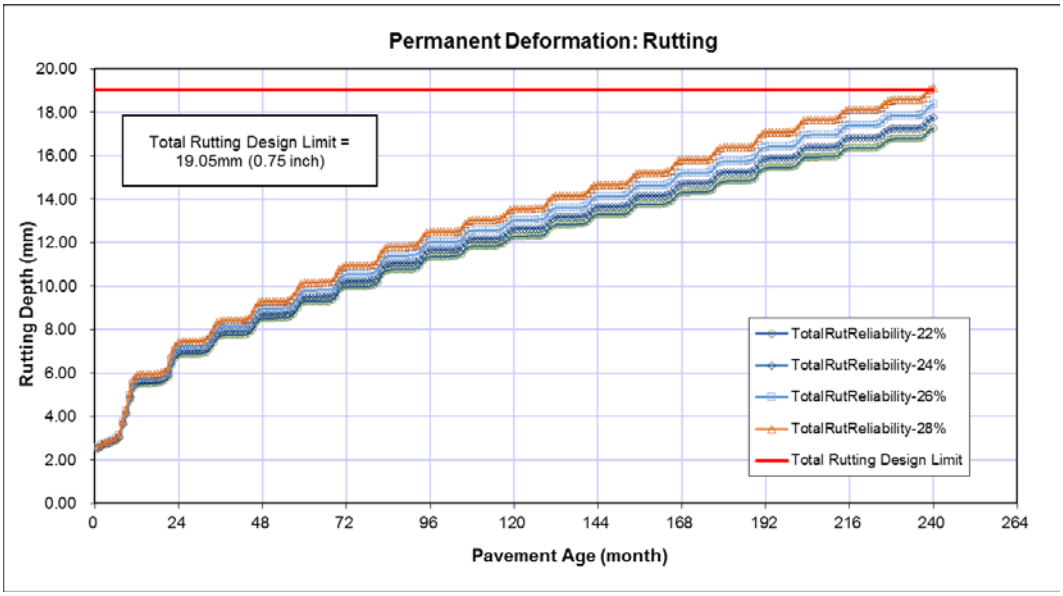

Figure 44. Predicted Rutting During 20-Year Service Life of Pavement with Above-Base Drainage Layer Having Different Air Void Contents (Idaho ATPB).

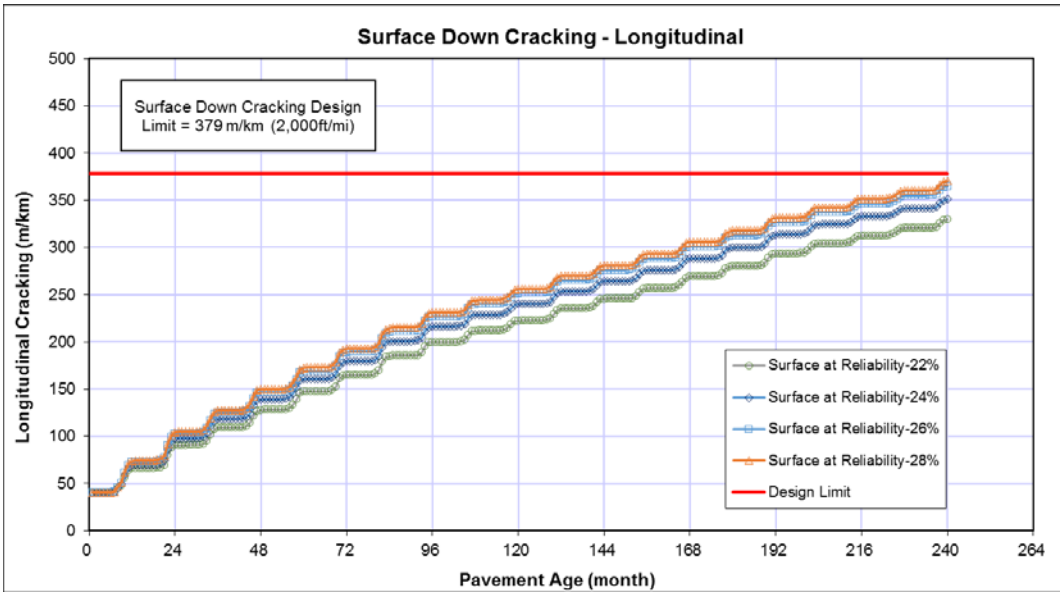

Figure 45. Predicted Surface-Down Cracking During 20-Year Service Life of Pavement with Above-Base Drainage Layer Having Different Air Void Contents (Idaho ATPB).

CONCLUSIONS

- When the VTM is greater than 24%, the difference in measured air void content between parafilm method and vacuum sealing method becomes significant. To determine which method should be applied first, an estimation of the air void content by the dimensional method can be used.

- During dynamic modulus testing of ATPB materials, modified stress levels and test temperatures were needed to reduce the risk of plastic deformation during testing.

- The modified NCHRP 1-37A model was used to predict the measured dynamic modulus of ATPB materials using materials and volumetric properties.

- Based on FEM simulation, placing the drainage layer below the aggregate base can slightly reduce the permanent deformation measured at the surface of the pavement.

- The drainage layer contributes to the structural capacity of the pavement; however, this contribution is limited.

- An optimal VTM can be calculated to balance the needs of permeability and stiffness by using a permeability requirement and limiting the predicted deterioration using ME Pavement design. Optimal VTMs were found to range between 24% to 30%, but may vary slightly for different pavement structures.

RECOMMENDATIONS

- The VTM of drainage layer materials having a permeability less than 24% should be assessed by the Parafilm method. The VTM of drainage layer materials having a permeability of greater than 24% should be assessed by the vacuum sealing method.

- Modified stress levels and test temperatures should be considered when conducting the dynamic modulus test on ATPB materials to reduce the risk of plastic deformation during testing.

- Agencies should consider designing and placing permeable drainage layers at optimal VTM levels to balance the needs of permeability and stiffness.

ACKNOWLEDGMENTS

The authors acknowledge the following state departments of transportation for their help in providing technical and financial support to the project TPF 5(229):

- Virginia Department of Transportation
- Wisconsin Department of Transportation
- Oklahoma department of Transportation
- Idaho Transportation Department

REFERENCES

1. Federal Highway Administration, *Drainable Pavement Systems, Participant Notebook, Demonstration Project 87*. Rep. FHWA-SA-92-008, FHWA, Washington, D.C., 1992.

2. Fwa, T.F., Tan, S. A., and Guwe, Y. K. Rational Basis For Evaluation And Design of Pavement Drainage Layers. In *Transportation Research Record 1772*. Transportation Research Board, Washington, D.C., 2001, pp. 174–180.

3. Rokade, S., Agarwal, P.K., and Shrivastava, R. Drainage And Flexible Pavement Performance. *International Journal of Engineering Science and Technology*, Vol. 4, 2012, pp. 1308.

4. Federal Highway Administration, *Construction of Pavement Subsurface Drainage Systems (Reference Manual)*. Rep. FHWA/IF-01/014, FHWA, Washington, D.C., 2002.

5. AASHTO T 312-12. Standard Method of Test for Preparing and Determining the Density of Hot-Mix Asphalt (HMA) Specimens by Means of the Superpave Gyratory Compactor. American Association of State and Highway Transportation Officials, Washington, D.C., 2012.

6. ASTM C192/C192M-12. Standard Practice for Making and Curing Concrete Test Specimens in the Laboratory. ASTM International, 2012.

7. AASHTO T 85-10. Standard Method of Test for Specific Gravity and Absorption of Coarse Aggregate. American Association of State and Highway Transportation Officials, Washington, D.C., 2010.

8. AASHTO T209-11. Theoretical Maximum Specific Gravity and Density of Hot-Mix Asphalt Paving Mixtures. American Association of State and Highway Transportation Officials, Washington, D.C., 2011.

9. Crouch, L.K., Copeland, A.R., Walker, C.T., Maxwell, R.A., Duncan, G.M., Goodwin, W.A., Badoe, D.A., and Leimer, H.W. Determining Air Void Content of Compacted Hot-Mix Asphalt Mixture. In *Transportation Research Record 1813*, Transportation Research Board, Washington, D.C., 2002, pp. 39-46.

10. Hall, K.D., Griffith, F.T., and Williams, S.G. Examination of Operator Variability for Selected Methods for Measuring Bulk Specific Gravity of Hot-Mix Asphalt Concrete. In *Transportation Research Record 1761*, Transportation Research Board, Washington, D.C., 2001, pp. 81-85.

11. Virginia Test Method – 84. Determining the Coefficient of Permeability of Open Graded Drainage Layer Material - (Physical Lab). Virginia Department of Transportation, Richmond, 2000.

12. OHD L-44. Method of Test for Measurement of Water Permeability of Compacted Paving Mixtures. Oklahoma Department of Transportation, Oklahoma City, 2004.

13. ASTM D 5084. Standard Test Methods for Measurement of Hydraulic Conductivity of Saturated Porous Materials Using a Flexible Wall Permeameter. ASTM International, 2010.

14. Kanitpong, K., Bahia, H. U., Benson, C. H., and Wang, X. Measuring and Predicting Hydraulic Conductivity (Permeability) of Compacted Asphalt Mixtures in the Laboratory. Transportation Research Board 82nd Annual Meeting, Washington, D.C., 2003.

15. AASHTO T 342-11. Standard Method of Test for Determining Dynamic Modulus of Hot-Mix Asphalt Concrete Mixtures. American Association of State and Highway Transportation Officials, Washington, D.C., 2011.

16. Ongel A. and Harvey J. Analysis of 30 Years of Pavement Temperatures Using the Enhanced Integrated Climate Model (EICM). Pavement Research Center, Institute of Transportation Studies, University of California, Berkeley, and University of California, Davis, 2004.

17. Diefenderfer, B. K. Moisture Content Determination and Temperature Profile Modeling of Flexible Pavement Structures. Ph.D. dissertation, Department of Civil and Environmental Engineering, Virginia Polytechnic Institute and State University, Blacksburg, 2002.

18. Mejias, M. and Rushing, J.F. Performance Evaluation of Military Airfield Pavement Drainage Layers. *International Journal of Pavement Research and Technology*, Vol.4, No.6, 2011, pp. 365-372.

19. Hunsucker, D. Q. and Meade, B. W. Subsurface drainage of highway pavements. Report KTC 97-8, University of Kentucky, Lexington, KY, 1997.

20. Webb, D., Sholar, G., Musselman, J., Upshaw, P., and Page, G. An Evaluation of Asphalt Treated Permeable Base. Report FL/DOT/SMO/07-511, FDOT, FL, 2007.

21. Maupin, G. W. Design and Construction of a New Asphalt Drainage Layer. Report VTRC 05-R11, VTRC, Charlottesville, VA, 2004.

22. Koroma, A. A. Evaluation of the Performance and Cost Effectiveness of Pavement Sections Containing Open-Graded Base Courses. Ph.D. dissertation, Department of Civil and Environmental Engineering, Michigan Technological University, Houghton, MI, 2011.

23. Havens, J. H. and Sharpe, G. W. Water under Pavements. Research Report UKTRP-83-13. University of Kentucky, Lexington, Kentucky, 1983.

24. Forsyth, R.A., Asphalt Treated Permeable Material - Its Evolution and Application. Report QIP 117, National Asphalt Pavement Association, Lanham, MD, 1991.

25. Zhou, H., Moore, L., Huddleston, J., and Gower, J. Free Draining Base Materials Properties, Final Report. Report FHWA-OR-RD-92-11, Oregon Department of Transportation, Salem, 1992.

26. Harvey, J., Tsai, B., Long, F., and Hung, D. CAL/APT Program-Asphalt Treated Permeable Base (ATPB): Laboratory Testing, Performance, Predictions, and Evaluation of the Experience of Caltrans and Other Agencies. Report FHWA/CA/OR-99/09, California State Dept. of Transportation, Sacramento, 1999.

27. Nokes, W. A., Harvey, J. T., du Plessis, L., Long, F., and Stolarski, P.J. Caltrans Accelerated Pavement Testing (CAL/APT) Program-Test Results: 1993-1996. In *8th International Conference on Asphalt Pavements*, Boston, MA, 1997, pp. 20.

28. Pologruto, M. Study of In-Situ Pavement Material Properties Determined from FWD Testing. *Journal of Transportation Engineering*, Vol. 132, No. 9, 2006, pp. 742-750.

29. Hall, K.T. and Crovetti, J.A., Effects of Subsurface Drainage on Pavement Performance Analysis of the SPS-1 and SPS-2 Field Sections, Report TRB/NCHRP/REP-583, Aptek, Inc., Colorado Springs, CO. Texas Transportation Inst., College Station, 2007.

30. Kozeliski, F.A., Permeable Bases Help Solve Pavement Drainage Problems. *Aberdeen's Concrete Construction*, Vol. 37, 1992, pp.660-662.

31. Loulizi, A., Al-Qadi, I. L. and Elseifi, M. Difference Between In-Situ Flexible Pavement Measured and Calculated Stresses and Strains. *Journal of Transportation Engineering*, Vol.132, No.7, 2006, pp. 574-579.

32. Al-Qadi, I. L, Loulizi, A., Lahouar, S., Flintsch, G.W., and Freeman, T. E. Quantitative Field Evaluation and Effectiveness of Fine Mix under Hot-Mix Asphalt Base in Flexible Pavement. In *Transportation Research Record 1823*, Transportation Research Board, Washington, D.C., 2003, pp. 133–140.

33. Khoury, N. N., Zaman, M., Ghabchi, R., and Kazmee, H. Stability and Permeability of Proposed Aggregate Bases in Oklahoma, Report FHWA-OK-09-05, The University of Oklahoma, Norman, 2010.

34. Witczak, M. Simple Performance Tests: Summary of Recommended Methods and Database. Report NCHRP-547, Transportation Research Board, Washington, D.C., 2005.

35. Winkelman, T. J., Open Graded Drainage Layer Performance in Illinois. Report FHWA/IL/PRR 147, Illinois State Dept. of Transportation, Springfield, 2004.

36. Idaho Transportation Department. Standard Specifications for Highway Construction, Boise, 2012.

37. Oklahoma Department of Transportation Commission. Standard Specifications for Highway Construction., Oklahoma City, 2009.

38. Virginia Department of Transportation. Road and Bridge Specifications, Richmond, 2007.

39. Wisconsin Department of Transportation. Standard Specifications for Highway and Structure Construction, Madison, 2014.

40. Witczak, M.W. and Bari, J. Development of A Master Curve (E*) Database for Lime Modified Asphaltic Mixtures. Department of Civil and Environmental Engineering, Arizona State University, Tempe, 2004.

41. Cross, S.A., Jakatimath, Y., and Sumesh KC. Determination of Dynamic Modulus Master Curves for Oklahoma HMA Mixtures. Report FHWA/OK 07 (05), Oklahoma Department of Transportation, Oklahoma City, 2007.

42. Kim, Y.R., Momen, M., and King, M. Typical Dynamic Moduli for North Carolina Asphalt Concrete Mixtures. Report FHWA/NC/2005-03, North Carolina Department of Transportation, Raleigh, 2005.

43. Timm, D.H., Turochy, R.E., and Davis, K.P. Guidance for M-E Pavement Design Implementation. ALDOT Project 930-685, Auburn University, Project 930-685, 2010.

44. Guide for Mechanistic-Empirical Design of New and Rehabilitated Pavement Structures. Appendix EE-1: Input Data for the Calibration and Validation of the Design Guide for New Constructed Flexible Pavement Sections. ARA, Inc., ERES Division. 2003.

45. Kutay, M.E. and Jamrah A. Preparation for Implementation of the Mechanistic-Empirical Pavement Design Guide in Michigan: Part 1-HMA Mixture Characterization. Report. RC-1593, Michigan State University, East Lansing, 2013.

46. American Concrete Pavement Association. Subgrades and Subbases for Concrete Pavements. Report ISBN 978-0-9800251-0-1, Skokie, IL, 2007.

47. Hadi, M. N. S. and Bodhinayake, B. C. Non-linear Finite Element Analysis of Flexible Pavements. *Advances in Engineering Software*, Vol. 34, No. 11-12, 2003, pp. 657-662.

48. Al-Qadi, I. L., Wang H., and Tutumluer, E. Dynamic Analysis of Thin Asphalt Pavements by Using Cross-anisotropic Stress-dependent Properties for Granular Layer. In *Transportation Research Record 2154*, Transportation Research Board, Washington, D.C., 2010, pp. 156-163.

49. Xiao, D. X., Hall, K. D., Wang, K. C. P. and Qiu, Yanjun. Long-term performance evaluation of permeable asphalt treated base in Arkansas. In *ICTE 2011 - Proceedings of the 3rd International Conference on Transportation Engineering*, Chengdu, China, 2011, pp. 2145-2150.

50. FHWA, (2009). TechBrief: Daylighted Permeable Bases [Online]. Available: http://www.fhwa.dot.gov/pavement/concrete/pubs/hif09009/

51. Xie, H. and Watson, D. E. Determining Air Voids Content of Compacted Stone Matrix Asphalt Mixtures. In *Transportation Research Record 1891*, Transportation Research Board, Washington, D.C., 2004, pp. 203-211.

APPENDIX A

COMPARATIVE AND STATISTICAL ANALYSIS OF AIR VOID CONTENT BY METHOD

The air void content obtained from the dimensional and parafilm methods on ATPB specimens from Virginia and Oklahoma indicated that the dimensional method usually yields higher air void content than the parafilm method as shown in Figure A1. It was found that for specimens with air void contents up to 30%, the as-compacted surfaces are rough and the specimen cannot be assumed as a solid cylinder. In this case the dimensional method which relies on the measured diameter and thickness to calculate the volume is unreliable while the parafilm method utilizing water replacement method could yield better results. The bulk specific gravity and the air void content of the CTPB materials from Oklahoma were determined by the vacuum sealing method.

A comparison between the vacuum sealing and parafilm methods showed that lower air void contents were obtained using vacuum sealing on more than 30 ATPB specimens from Oklahoma as in Figure A2. It was also found that the differences between methods increased with increasing air void content. Using the vacuum sealing method, the plastic bag was found to lie more tightly around the specimen surface than the parafilm and consequently the volume obtained was thought to be closer to the actual volume.

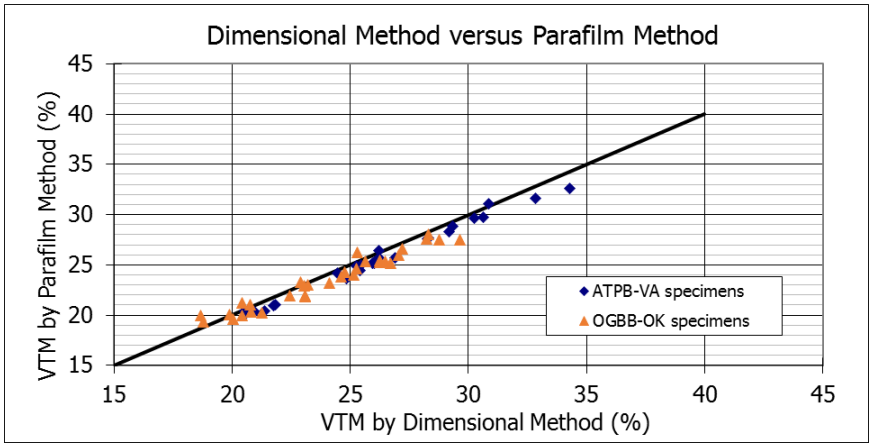

Figure A1. Relationship of the Air Void Content Obtained from Dimensional and Parafilm Methods.

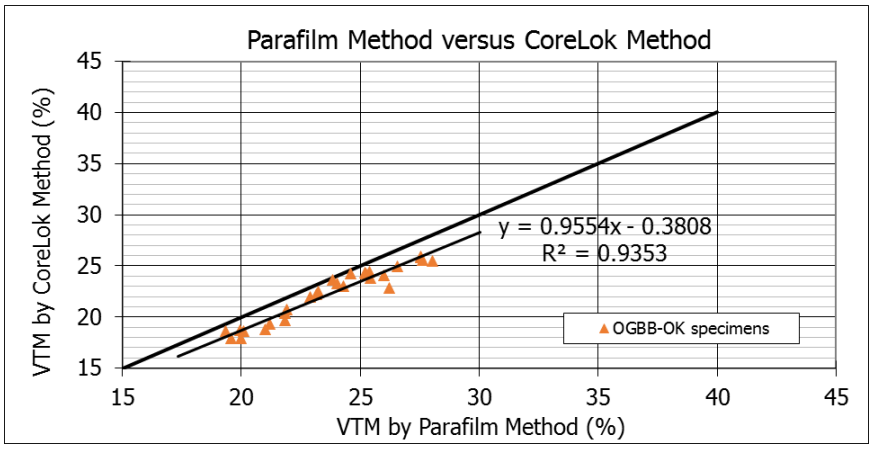

Figure A2. Relationship of the Air Void Content obtained from Parafilm and CoreLok Methods.

Based on statistical analyses of the air void content determined by the three methods on about 30 specimens, the coefficient of variance (CV) of the vacuum sealing method is the least while the dimension method has the greatest CV as shown in Table A1. Therefore the vacuum sealing method is believed to be a more repeatable procedure with less variation than other methods used in this study.

Table A1. Statistical Analysis of Air Void Content Determined by Three Methods

Method	Mean	Standard Deviation	Coefficient of Variance
Dimensional	23.205	3.188	13.740
Parafilm	23.343	2.912	12.477
Vacuum Sealing	21.465	2.575	11.996

According to a previous study by Xie et al., there is a system error for the vacuum system method when testing specimens with low air void content, and this error should be accounted for on each piece of equipment.[51] However, considering the specimens used in this study are of air void content larger than 20%, no correction was applied.

An ANOVA was also conducted to confirm whether the difference between the air void content obtained from the three methods is statistically significant. The results in Table A2 show that the difference in air void content between the three methods is not statistically significant; the *P*-value was 0.0647 (greater than 0.05 indicates no significance at 95% confidence). However, when considered individually, the difference in air void content between the parafilm method and the vacuum sealing method was found to be significant; the P-value was 0.0357 (less than 0.05 indicates significance at 95% confidence).

The results in Table A3 show that the testing method adopted to determine the air void content can influence the results significantly. Therefore each method has its own applications and should only be adopted within certain VTM ranges to obtain good results and improve time and cost efficiency. The ANOVA analysis reveals that for specimens of larger than 21% VTM, significant difference exists among the three methods or within each pair of two methods based on 95% confidence. With a decrease in the air void content from 25% to 20%, the differences

among the three methods or between each two of the methods become less significant, with no significant difference observed on specimens with 20% or less air void content.

Table A2. Analysis of Variance

Source	**Degrees of Freedom**	**Sum of Squares**	**Mean Squares**	**F Ratio**	**Probability > F**
Methods	2	48.21675	24.1084	2.8612	0.0647
Error	63	530.84348	8.4261		
Total	65	579.06023			
Level	**Difference**	**Standard Error of Difference**	**Lower Confidence Level**	**Upper Confidence Level**	**P-Value**
Parafilm vs. Vacuum	1.878363	0.8752188	0.12938	3.627348	0.0357
Dimensional vs. Vacuum	1.740006	0.8752188	-0.00898	3.488991	0.0512
Parafilm vs. Dimensional	0.138357	0.8752188	-1.61063	1.887342	0.8749

Table A3. Statistical Test on Three Methods in Accordance to VTM

Group	**P value**			
	F test	**T test**		
	Dimensional & Parafilm & CoreLok	**Dimensional & Parafilm**	**Parafilm & CoreLok**	**Dimensional & CoreLok**
>25%	0.0006*	0.6251	0.0053*	0.0007*
>24%	0.0041*	0.6759	0.0307*	0.0042*
>23%	0.0181*	0.7313	0.0942	0.0175*
>22%	0.0262*	0.7816	0.1137	0.0260*
>21%	0.0742	0.6696	0.0813	0.0319*
>20%	0.0742	0.9036	0.1869	0.0796

* indicates there is a significant difference based on 95% confidence.

When the VTM is greater than 24%, the difference between parafilm method and vacuum sealing method becomes significant. Therefore, in laboratory testing, the dimensional method can be used for specimens of less than 21% VTM and Parafilm method is good to test specimens of less than 24% VTM, for the sake of cost efficiency. The CoreLok method should be applied for specimens of VTM larger than 24%. To determine which method should be applied first, an estimation of the air void content by the dimensional method can be used. However, in practice, there may be large variations between the real and target air void content, or the batches of specimens have wide ranges of air void contents. In this case, it is more important to conform to a consistent test method, and the CoreLok vacuum sealing method is preferable.

The recommended steps to determine the choice of test method for drainage layer materials are shown below. Firstly, the rough ranges of the air void content should be estimated. If the air void contents are with small variation all below 24%, the Parafilm method can be adopted. This situation is more common in laboratory test on laboratory-compacted specimens. Once there is a specimen with air void content exceeding 24%, the vacuum sealing method should be applied on all specimens to facilitate comparison. In this study, the VTM used in further data analysis were determined by appropriate test methods as recommended here.

APPENDIX B

DYNAMIC MODULUS OF ATPB MATERIALS

The average dynamic modulus of the ATPB materials from each state at the 10 Hz test frequency are shown in Table B1.

Table B1. Average Dynamic Modulus of ATPB Materials at 10 Hz

	Specimen	4.4ºC	12.7ºC	21.1ºC	29.4ºC	37.8ºC
Virginia	20% VTM	7612.289	5309.411	3730.375	2673.110	1598.813
	21% VTM	8566.412	5409.16	3783.761	2752.11	1621.786
	24% VTM	5442.765	3875.09	2696.169	1663.091	1040.927
	25% VTM	5597.803	3235.746	2183.735	1382.885	801.8873
	26% VTM	5074.623	3190.896	2264.236	1378.151	808.9129
	28% VTM	4322.767	2548.123	1762.647	1136.652	516.3588
Oklahoma	18% VTM	6070.078	4953.639	3963.297	2952.423	1782.701
	19% VTM	5913.067	4865.333	3921.023	2888.564	1674.506
	20% VTM	5895.158	4683.611	3190.204	2533.586	1536.657
	22% VTM	5997.318	4765.427	3445.269	2708.969	1593.641
	23% VTM	5444.044	3909.738	3188.991	2304.592	1693.905
	24% VTM	5607.72	4807.467	3385.209	2522.644	1515.907
	25% VTM	5693.037	4296.393	3044.458	2280.54	1366.924
	26% VTM	4369.521	3517.003	2709.274	1915.487	1182.307
Idaho	22% VTM	5150.747	3678.842	2231.781	1372.764	736.5299
	24% VTM	4499.202	3073.779	1705.456	1033.836	549.3619
	25% VTM	4420.531	3072.392	1640.484	881.9722	N/A
	26% VTM	4056.224	2531.278	1376.974	631.2243	N/A
	28% VTM	2773.239	1841.138	1008.255	N/A	N/A

APPENDIX C

DEM SIMULATION TO PREDICT THE RESILIENT MODULUS OF UPB

The Discrete Element Method (DEM) is one of the numerical methods to simulate the movement and interaction of a large number of particles such as the UPB. It has been widely applied to solve engineering problems related with discontinuous and granular materials such as rocks and sands. In this study, the three dimensional discrete element code, PFC^{3D} was used to investigate the resilient behavior of the high-porosity unbound open-graded drainage layer materials under cyclic axial loadings, which may require tremendous efforts to be determined through laboratory test.

DEM Numerical Modeling

In DEM simulation, a contact occurs when two particles interact with each other causing forces on them. There are several kinds of contact mode in PFC^{3D}, among which the linear contact-stiffness model is one of the most simple contact models. Considering the materials that needed to be simulated are unbound, and the resilient modulus test applies exclusively compressive stresses only leading to small stress-strain conditions, the linear model is adequate to solve the problem. Therefore, the linear contact-stiffness model was adopted to relate the normal and shear components of force and the relative displacement in this study. Equations C.1 and C.2 give the constitutive relationship in the linear contact-stiffness model.

$$F_i^n = K^n U^n n_i \tag{C.1}$$

$$\Delta F_i^s = -k^s \Delta U_i^s \tag{C.2}$$

Where

F_i^n is the i th component of the total normal force;
K^n is the normal stiffness or secant stiffness;
U^n is the total normal displacement;
n_i is the vector in the i th direction;
ΔF_i^s is the i th component of the increment of shear force;
k^s is the shear stiffness or tangent stiffness; and
ΔU_i^s is the i th component of the increment of shear displacement.

When two particles are in contact with each other, the contact stiffness K^n and k^s are function of the properties of the two particles, as shown in Equations C.3 and C.4.

$$K^n = \frac{k_n^{[A]} k_n^{[B]}}{k_n^{[A]} + k_n^{[B]}} \tag{C.3}$$

$$k^s = \frac{k_s^{[A]} k_s^{[B]}}{k_s^{[A]} + k_s^{[B]}} \quad \text{(C.4)}$$

Where the superscripts [*A*] and [*B*] denote the two particles in contact.

The Servomechanism to Realize Cyclic Loadings

The resilient modulus is the property of a material under repeated cyclic loadings. In pavement analysis, the repeated cyclic loading is the most similar loading form as real traffic loading and the resilient modulus is considered to be one of the representative mechanical properties to consider the pavement responses. To investigate the resilient modulus of unbound drainage materials, the numerical servomechanism in FISH codes have been applied to control the speed and position of confining walls to maintain required confining and axial stresses on the specimen. The confining pressure is maintained throughout the simulation to be a constant value as much as possible, and the axial stress is set to be repeated loading-unloading conditions. Equations C.5 and C.6 show the servo-controlled velocities of the walls to achieve specified confining and axial stresses.

$$\dot{u}^{(w)} = \mathrm{G}\left(\sigma^{measured} - \sigma^{required}\right) = G\Delta\sigma \quad \text{(C.5)}$$

$$\mathrm{G} = \frac{\alpha A}{k_n^{(w)} N_c \Delta t} \quad \text{(C.6)}$$

Where

$\dot{u}^{(w)}$ is the wall velocity;
G is the gain parameter;
$\sigma^{measured}$ and $\sigma^{required}$ are the measured and required stresses on the wall;
α is the relaxation factor;
A is the wall area;
$k_n^{(w)}$ is the normal stiffness of the wall;
N_c is the number of contacts on the wall; and
Δt is the time increment.

Input Parameters

To obtain realistic simulation results, the gradation of the numerical specimen is selected based on the typical gradation of the Wisconsin UPB materials. The gradation of the numerical model is shown in Table 2. Figure C1 shows the specimen of the typical gradation with 45% air void content before loading and Figure C2 presents the contact force after the cyclic loadings.

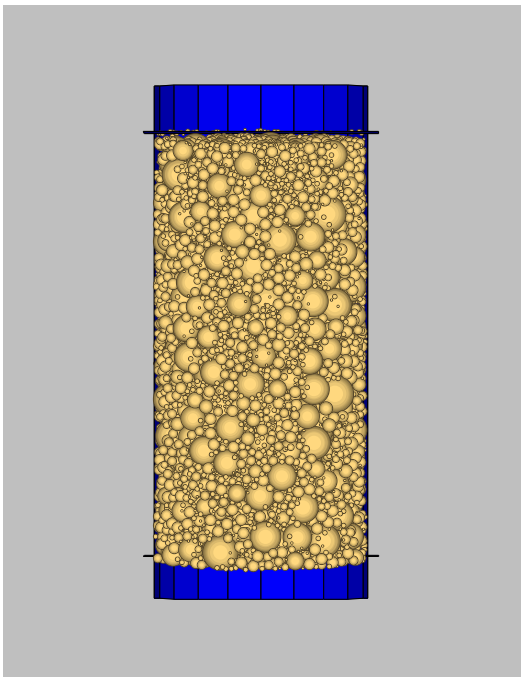

Figure C1. Specimen with 45% air void content before loading-unloading process.

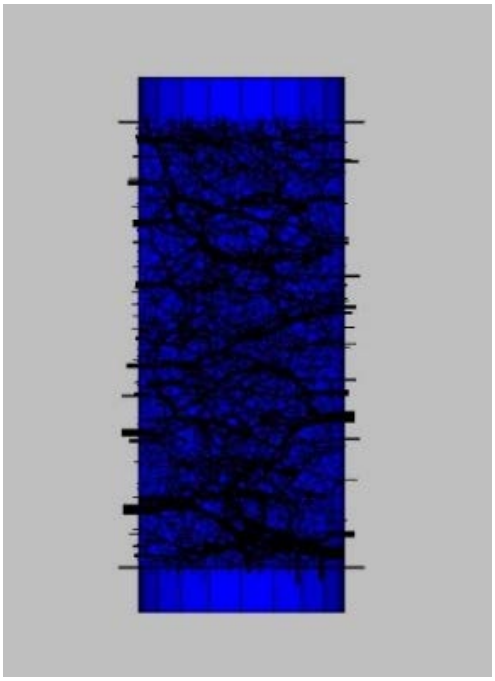

Figure C2. Specimen with 45% air void content and the contact force after loading-unloading process.

The target confining pressure and axial compressive pressure specified in the simulation are -1.379×10^5 and -2.482×10^5 Pa, respectively, which are selected according to the loading sequence in AASHTO T307 standard. However, during the simulation, the confining and axial pressures fluctuate around the target values and are not strictly the same as the target pressures.

The real confining and axial pressure during the calculation were recorded and are presented in the part of results and discussions.

DEM simulation on resilient modulus of UPB for Wisconsin

Initial air void content of 45%

As stated previously, during the loading-unloading process, the required confining pressure and axial pressure were specified. The top plate and the cylindrical surface were assigned instant speeds to reach or keep the specified confining and axial pressure. At the beginning of loading, the cylindrical wall was fixed and the top plate was moved downward at constant speed. As the confining pressure increased to the required value, "servo" control was turned on to adjust the speeds of the top plate and the cylindrical wall to keep the required stress. As a result, during the first cycle of loading-unloading, the whole system was still under adjustment and had not reached required conditions. Therefore the data from the first cycle hasn't been included in the analysis. Figure C3 shows the stress-strain relationship during the second to the ninth cycles of the loading-unloading process on specimens with initial air void content of 45%.

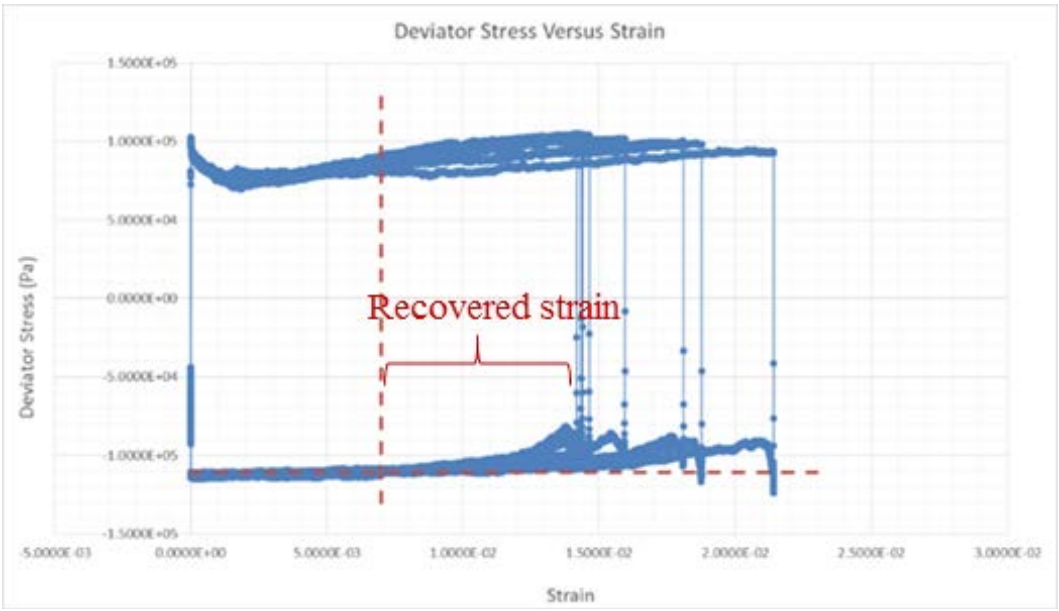

Figure C3. Relationship Between Stress and Strain Based on DEM Simulation at 45% Air Void Content.

From Figure C3, it can be found that the areas of the stress-strain hysteresis loops vary in each cycle. At the beginning, from the first to fourth cycle, the same loading caused larger strain within the same loading time. As a result, the area of the hysteresis loop is larger than that during the sixth to ninth cycles. As the specimens underwent several cycles of axial loading, the specimens were compacted and the strains caused by the loading began to stabilize around 0.014, as can be observed from Figure C3. The last five hysteresis loops have been used to calculate the resilient modulus of the unbound open-graded materials.

The initial condition was set to be the left bottom point of the hysteresis loops as shown in Figure C3. At this point, the deviator stress and the axial stress reached stable minimal values during the unloading period, which also marked the end of the last unloading period and the beginning of the next loading period. At the unloading stage, it was assumed that when the stress on the top surface reached this initial condition and kept stable values around it, the unloading condition had been achieved. The red vertical dash line shows where the unloading process finished. The resilient modulus of the sample with 45% air void content calculated from the last five cycles is as Equation C.7:

$$M_r = \frac{Deviator\ stress}{Recovered\ strain} = \frac{1.0585\times10^{5}}{1.450\times10^{-2}-7.000\times10^{-3}} = 14.1MPa \quad (C.7)$$

Influence of the initial air void content

To investigate the influence of the air void content, specimens with initial air void content of 41% and 48% were constructed and tested for the resilient modulus in PFC3D. The required confining stress and axial loading were maintained as the same in the case when the initial air void content of the specimen was 45%. The stress-strain relationship during the second to the ninth cycles of loading-unloading process on specimens with initial air void content of 41% and 48% are presented in Figure C4 and Figure C5.

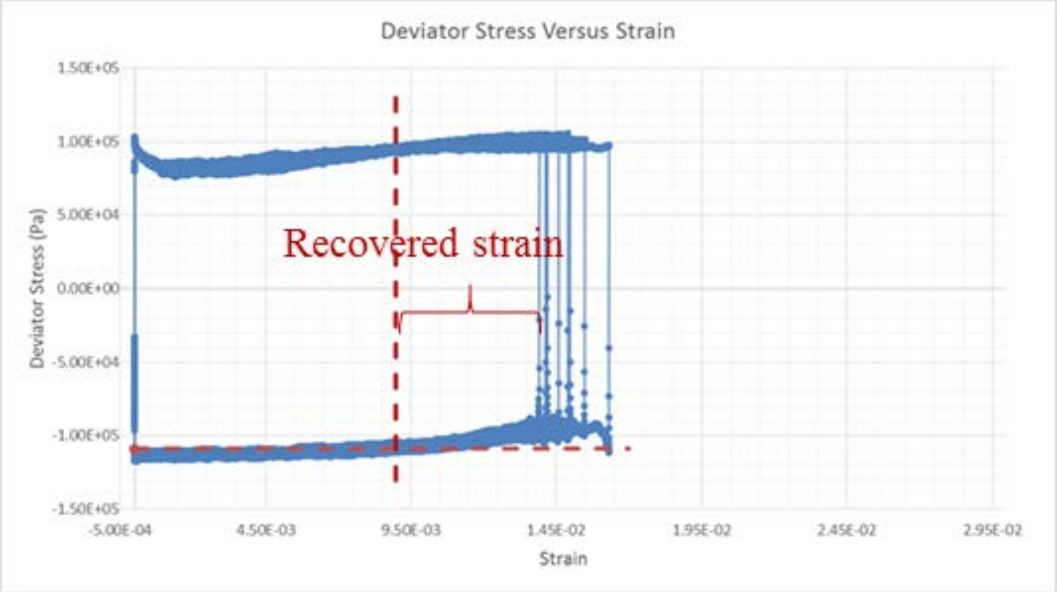

Figure C4. Relationship Between Stress and Strain Based on DEM Simulation at 41% Air Void Content.

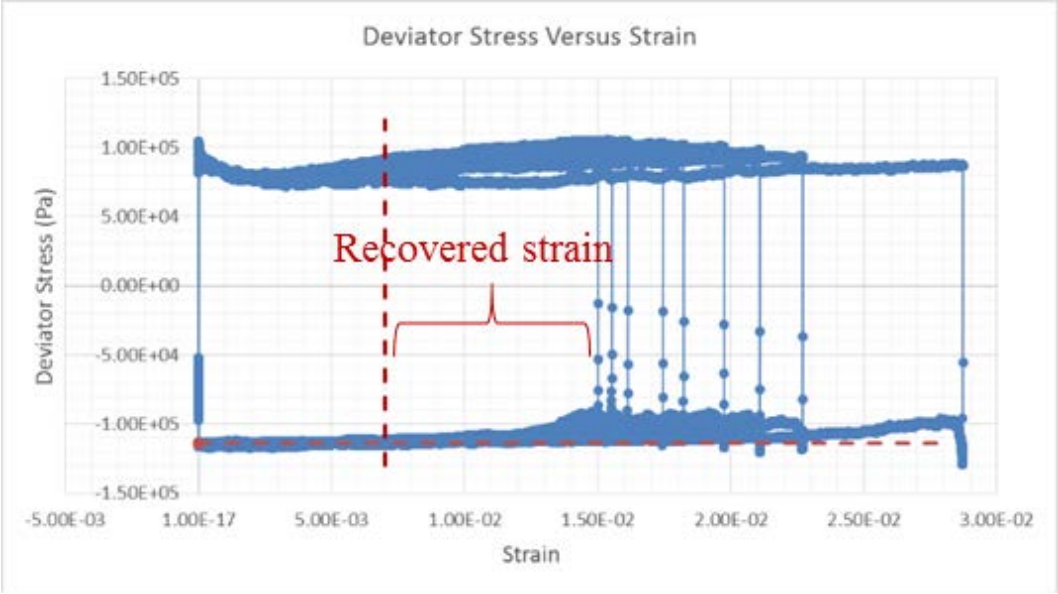

Figure C5. Relationship Between Stress and Strain Based on DEM Simulation at 48% Air Void Content.

The maximum and minimum values in Figures C3 and C4 are set to be the same to facilitate comparison. From these figures, it can be found that in both cases the areas of the stress-strain hysteresis loops vary in each cycle. However, when the air void content is 41%, the difference between the areas of the stress-strain hysteresis loops are not as significant as that when the air void content is 45%. At the first loop, the strain developed in specimen with 45% air void content is much larger than the strain developed in the sample with 41% air void content, even though the axial stresses are at the same level. This can be attributed to the initial state of the samples. The sample with larger initial air void content is more easily compacted and obtains larger strains. After ten cycles of the loading-unloading process, the system gradually reached stable status with small-changed strains. Finally the systems achieved very similar status at the end of the tenth cycle no matter the initial air void content, 41% or 45%. The strains of the two samples with 41% and 45% air void content in the last five loops are also very similar. These findings can also be verified from comparing the stress-strain relationship between samples of 45% and 48% initial air void content.

The last five hysteresis loops have been used to calculate the resilient modulus of the unbound open-graded materials with 41% and 48% initial air void content are shown as Equations C.8 and C.9, respectively:

Sample having 41% air void content:

$$M_r = \frac{Deviator\ stress}{Recovered\ strain} = \frac{1.0588\times10^{5}}{1.390\times10^{-2}-9.000\times10^{-3}} = 21.608MPa \quad (C.8)$$

Sample having 48% air void content:

$$M_r = \frac{Deviator\ stress}{Recovered\ strain} = \frac{1.0491\times10^{5}}{1.5006\times10^{-2}-7.000\times10^{-3}} = 13.104MPa \quad (C.9)$$

Based on the DEM simulation, it shows that the resilient modulus of the sample with 45% air void content is 14.1 MPa, only slightly larger than the resilient modulus of sample with 48% air void content which is about 13.1 MPa. The calculated resilient modulus of the sample with 41% air void content is about 6 MPa greater. In fact, although the difference between the last five cycles is not significant, the calculated resilient moduli still might be relatively smaller than the true values for the sample with 45% or 48% initial air void content under 10 loading cycles. The sample with 48% air void content approached the stable status as the stress-strain hysteresis shrunk until the tenth cycle. Therefore the resilient moduli obtained from the DEM simulation presented here are conservative compared with the laboratory-determined values. Figure C6 plots the relationship between resilient modulus and air void content obtained from both laboratory test and DEM simulation.

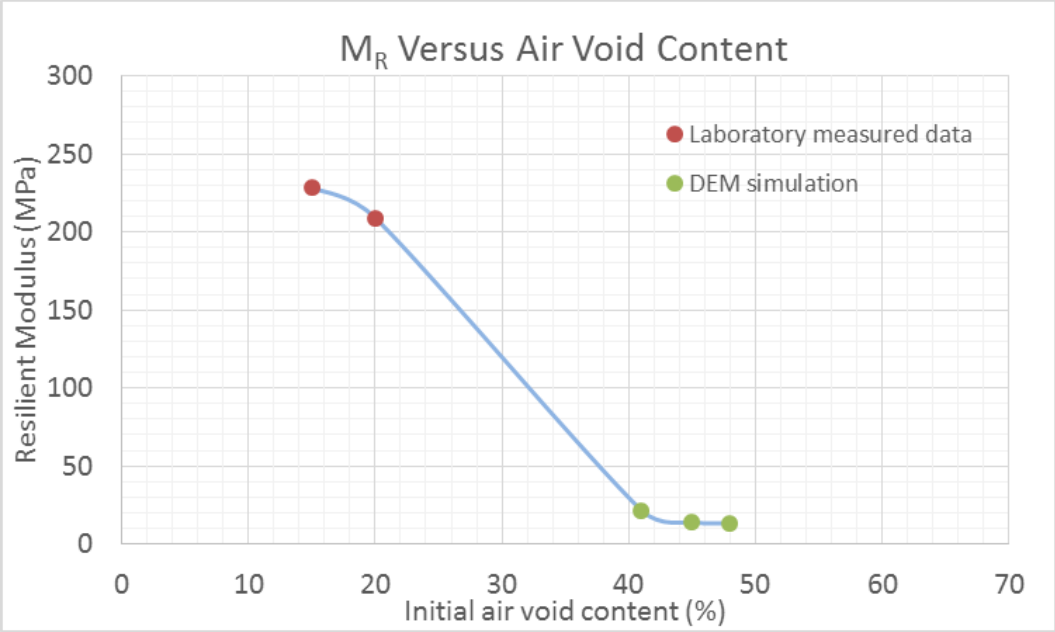

Figure C6. Resilient Modulus Versus Initial Air Void Content Using Data from Laboratory Test and DEM Numerical Calculation.

As can be seen from Figure C6, the resilient modulus of unbound open-graded drainage layer material is relatively small compared with regular unbound base material, and decreases with increasing air void content.